biomass

MDPI

Article

Synthesis of Biomass-Derived Polyurethanes with Film Formation: Kraft Lignin-Hydroxyalkylated or Not, and Ricinoleic Acid Triglyceride as Polyols

Ana Ribeiro Cassales [1,2], Diego Beltrame Pereira [1], Deyvid de Souza Porto [1], Luiz Antonio Ramos [1] and Elisabete Frollini [1,*]

[1] Macromolecular Materials and Lignocellulosic Fibers Group, Center of Research on Science and Technology of BioResources, Institute of Chemistry of São Carlos, University of São Paulo, São Carlos 13566-590, São Paulo, Brazil; ana.cassales@embrapa.br (A.R.C.); diego_beltrame@usp.br (D.B.P.); deyvid.porto@gmail.com (D.d.S.P.); ramos@iqsc.usp.br (L.A.R.)

[2] Embrapa Instrumentation, São Carlos 13561-206, São Paulo, Brazil

* Correspondence: elisabete@iqsc.usp.br

Abstract

A significant amount of Kraft lignin (KL) is produced each year, but only a small portion is repurposed to create higher-value products. KL was purified (PKL, ≈2300 g/mol, 4.1 mmol/g total OH) and used as a polyol in the synthesis of polyurethanes (PUs). It was also hydroxyalkylated with glutaraldehyde (PKL-Glu, ≈4400 g/mol, 5.8 mmol/g total OH). Ricinoleic acid triglyceride (a major component of castor oil, CO) was used as an additional source of hydroxyl groups (30/70 and 50/50 as PKL or PKL-Glu/CO ratio), and polymeric methylene diphenyl diisocyanate served as a source of isocyanate groups. The reaction mixture was spread on a glass plate using an extender (0.5 mm) in the absence of solvent and catalyst, and films were formed simultaneously with synthesis at 25 °C, 50 °C, 75 °C, and 100 °C. The films formed at 25 °C showed lower crystallinity than the others, especially the 50/50 PKL-Glu/CO product (13%), and lower hydrophobic character. Except for the 50/50 PKL-Glu/CO series, the others exhibited Tg for the flexible and rigid phases. The parameter that most impacted the tensile properties was the PKL or PKL-Glu/CO ratio. For example, films formed at 100 °C, when the ratio changed from 30/70 to 50/50, showed tensile strength/elongation/Young's modulus changing from 15 MPa/36%/271 MPa to 25 MPa/5%/1137 MPa (from PKL), and from 16 MPa/54%/250 MPa to 33 MPa/6%/1361 MPa (from PKL-Glu). Using KL, derivatized or not, as a polyol in the synthesis of PUs via a scalable, sustainable process can yield films with a range of properties modulated by various parameters, with potential applications in packaging, automotive interiors, and coatings for electronics, among others.

Keywords: Kraft lignin; hydroxyalkylation; glutaraldehyde; bio-based polyurethane synthesis; simultaneous film formation

Check for updates

Academic Editor: Miguel Angel Centeno

Received: 4 August 2026
Revised: 11 September 2026
Accepted: 16 September 2026
Published: 21 September 2026

Copyright: © 2026 by the authors. Licensee MDPI, Basel, Switzerland. This article is an open access article distributed under the terms and conditions of the Creative Commons Attribution (CC BY) license.

1. Introduction

Researchers have extensively investigated the use of renewable reagents in polyurethanes (PUs) as a strategy to reduce dependence on fossil-derived raw materials. PUs are a class of polymeric materials whose properties can be tailored by the chemical nature and functionality of their constituents, enabling applications across several sectors, including automotive, textiles, civil engineering, and biomedical fields [1]. Among renewable resources, lignin

has attracted particular interest as a potential polyol for PU synthesis because of its abundance and the presence of hydroxyl functional groups in its structure, particularly alcoholic hydroxyl groups [2]. These functionalities enable the partial or complete replacement of fossil-derived diols or polyols conventionally employed in the production of PUs [3–9]. Furthermore, lignin is the second most abundant plant macromolecule after cellulose [9,10]. Its widespread availability and renewable origin make it an attractive feedstock for developing bio-based polymeric materials [11].

Lignin has therefore been investigated as a renewable polyol for several types of PUs, including foams, adhesives, coatings, elastomers, and films [12]. The hydroxyl groups in its structure react directly with isocyanates, enabling partial substitution of conventional fossil-based polyols. However, incorporating lignin into PU networks remains challenging because lignin is a structurally heterogeneous macromolecule whose chemical characteristics depend strongly on both the biomass source and the extraction process [9]. In particular, lignin commonly contains a considerable proportion of phenolic hydroxyl groups, which react less readily with isocyanates than aliphatic hydroxyl groups. Its relatively high molar mass, heterogeneous functionality, and steric effects may further limit its reactivity and influence polymerization kinetics, phase organization, and the resulting PU properties [13].

Consequently, several lignin-modification strategies have been investigated to overcome these limitations, including phenolation [14], etherification–oxypropylation [4], and hydroxyalkylation [15]. These approaches can modify lignin's molecular structure and increase the availability or accessibility of hydroxyl groups for subsequent reaction with isocyanates. Among them, hydroxyalkylation is particularly attractive because it can alter lignin's functionality while maintaining its aromatic structure. Strategies to increase the content or accessibility of aliphatic hydroxyl groups are especially relevant, given their higher reactivity toward isocyanates than phenolic hydroxyl groups [5,13,16].

Hydroxyalkylation of lignin has commonly been investigated using aldehyde-based reagents [15]. In the present approach, lignin was reacted with glutaraldehyde, which is less volatile than other aldehydes, to introduce additional aliphatic hydroxyl groups into the lignin structure (Figure 1). Glutaraldehyde is a dialdehyde that can react at multiple aromatic ring sites on the lignin molecule; its bifunctional nature significantly increases the number of alcoholic hydroxyl groups relative to monoaldehydes. This increase enhances lignin's reactivity toward isocyanates and may influence the performance of the resulting polyurethanes. In addition, glutaraldehyde is a five-carbon dialdehyde with an aliphatic carbon chain that serves as a flexible spacer between lignin macromolecules and can influence the properties of the resulting materials.

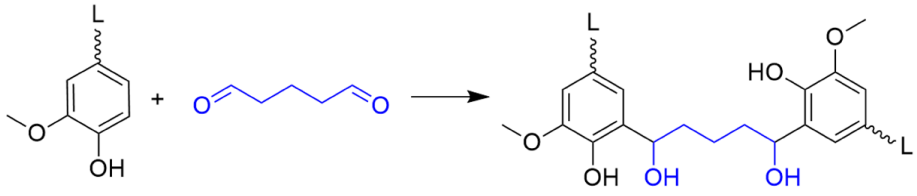


Figure 1. Representation of the hydroxyalkylation reaction of lignin with glutaraldehyde, focusing on the available positions on the aromatic rings.

Kraft lignin (KL) was selected as the lignin feedstock in this study. KL is the most widely produced technical lignin and is predominantly generated as a by-product of the Kraft pulping process in the pulp and paper industry [17]. It is estimated that 80 million tons of KL are generated each year globally, with most of this material used for energy recovery [17]. In contrast, only about 2% is repurposed to develop higher-value-added

products [18]. Therefore, incorporating KL into bio-based polymeric materials offers an opportunity to increase the value of this abundant industrial by-product.

In a previous study [19], unmodified KL was successfully employed as a polyol for the solvent- and catalyst-free synthesis of LignoPU polyurethanes with simultaneous film formation. In that approach, ricinoleic acid triglyceride, the primary component of castor oil [20,21], was also incorporated as a renewable hydroxyl-containing component. In addition to contributing hydroxyl groups to the formulation, castor oil played an important role in processing and dispersing KL, particularly because polymeric methylene diphenyl diisocyanate (pMDI), the other reactive component, is highly viscous. Although unmodified KL can be incorporated directly into LignoPUs, modifying its functionality may offer an additional way to control reactivity and the resulting macromolecular organization. PUs synthesized with chemically modified lignin as a polyol may yield materials with properties different from those of unmodified lignin derivatives.

For lignin-based PU films, reported synthesis approaches commonly involve combining synthetic polyols, such as polyethylene glycol [22–24], catalysts, and solvents [25–28]. The resulting films are predominantly prepared by casting, which involves dissolving or dispersing the polymer in a solvent, followed by solvent evaporation to form the film [29]. This study explored the properties of films formed using KL, a renewable polyol, in solvent- and catalyst-free reactions conducted at 50, 75, and 100 °C, with simultaneous film formation, which is an advantageous process compared to casting, since the synthesis of the PU and the formation of the film occur in a one-pot process. Conversely, as far as is known, no reports combine lignin hydroxyalkylation synthesis of polyurethanes (PUs) that simultaneously form films while also addressing the effect of synthesis temperature on LignoPU properties and the use of high lignin content as a macromonomer in the synthesis. In this context, this study evaluates unmodified KL and hydroxyalkylated KL as renewable polyols. The effects of chemical lignin modification and synthesis temperature on the properties of the resulting material were investigated to clarify their roles in the structure-property relationships of the resulting films. This study examined new parameters related to the topic, adopting conditions that enhance the scalability and industrialization of more sustainable processes.

2. Materials and Methods

2.1. Materials

Glutaraldehyde (50–51.5% *w*/*v* aqueous solution) was obtained from Êxodo Científica (Sumaré, São Paulo, Brazil) and used without further purification. Toluene P.A.—A.C.S (minimum content 99.5%) and potassium hydroxide (KOH, minimum content 85%) were acquired from Synth (Diadema, São Paulo, Brazil).

KL, derived from Eucalyptus, was supplied by Suzano Pulp and Paper (Limeira, São Paulo, Brazil). As presented in a previous study [19], after assessing various purification methods for the received KL, distilled water was ultimately selected as the solvent at a 1:10 KL-to-water ratio, and the mixture was heated at 70 °C for 1 h, aiming to eliminate contaminants such as inorganic salts and low molecular weight hemicellulose fragments. This choice was made for its simplicity and cost-effectiveness. Experiments were conducted for durations exceeding one hour. However, the mass differences between the starting and purified lignin were similar to those observed at one hour, indicating that this time is sufficient to remove water-soluble contaminants. After purification, the solution was filtered and dried in a circulating-air oven at 105 °C until it reached a constant weight.

Polymeric methylene diphenyl diisocyanate (pMDI, Desmodur® VP PU 0129 M, containing 33.6% NCO groups) was provided by Covestro (São Paulo, Brazil).

Castor oil (CO) primarily reflects the properties of its major component, the triglyceride of ricinoleic acid. According to the supplier (Azevedo Indústria e Comércio de Óleos Ltd.a., Itupeva, São Paulo, Brazil), the hydroxyl index is 155 mg KOH g^{-1} and the number-average molar mass (Mn) is 980 g mol^{-1}.

2.2. PKL Hydroxyalkylation

Glutaraldehyde (Glu), PKL, and KOH were mixed in a mass ratio of 1:2:0.075 and homogenized by mechanical stirring for 60 min in a reaction flask [30]. The reaction medium pH was approximately 9.5. The temperature was raised to 70 °C and held for 1 h, then increased to 95 °C for an additional 2 h. After cooling the system, the pH was adjusted to 5 with a 10% *w*/*v* HCl solution. Toluene was added to the medium at a 1:1 (*v*/*v*) ratio, and agitation was maintained for 2 h to promote the precipitation of the modified PKL, referred to as PKL-Glu. The PKL-Glu was then filtered, thoroughly washed with distilled water, and dried to a constant weight in a circulating-air oven at 105 °C.

2.3. LignoPUs Synthesis with Simultaneous Film Formation

Figure 2 shows the synthesis of LignoPUs with simultaneous film formation, using pMDI as the isocyanate source.

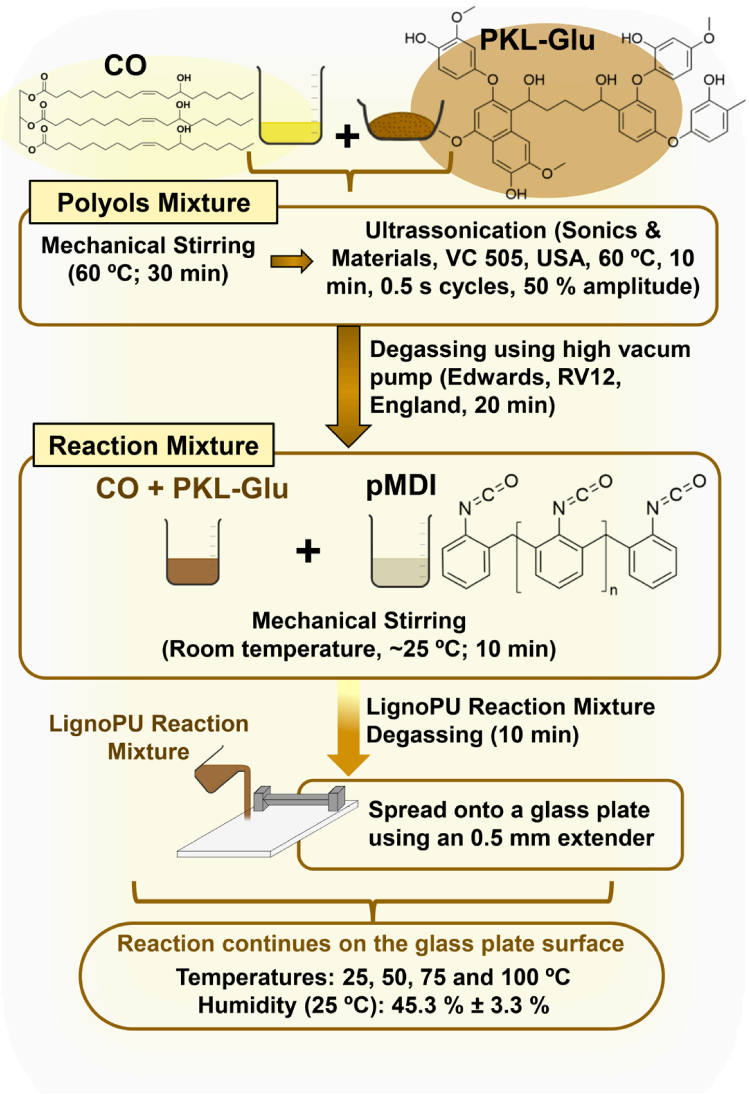


Figure 2. Synthesis scheme of LignoPUs with simultaneous film formation.

In the syntheses outlined in Figure 2, masses were determined stoichiometrically to ensure a 1:1 ratio of OH to NCO groups. The hydroxyl group content of each polyol was adjusted to achieve the specified 30/70 and 50/50 ratios for PKL-Glu (or PKL) and CO, respectively. The hydroxyl group content of PKL-Glu was quantified by elemental analysis and proton nuclear magnetic resonance (^{1}H NMR), as outlined in Section 2.4.1.

Hydroxyl group sources (CO, PKL, or PKL-Glu) were mechanically stirred for 30 min, then ultrasonicated for 10 min at 60 °C. The resulting mixture was then combined with pMDI at room temperature. This step was intended to control the reaction onset and achieve the appropriate viscosity for spreading the mixture onto a glass plate. The reaction sequence on the plate was conducted at 25 °C, with 25 °C increments (50 °C, 75 °C, and 100 °C), to evaluate the influence of reaction temperature on the properties of the formed films.

The reaction mixtures were spread onto glass plates and placed either in a controlled-temperature (25 °C), controlled-humidity environment or in an oven with air circulation at 50 °C, 75 °C, or 100 °C (Figure 2). FTIR spectra showed that isocyanate groups were consumed in all experiments, yielding solid films.

Control films were prepared using PKL as the polyol in PU synthesis, rather than PKL-Glu, following the method outlined in Figure 2. Results for films with PKL/CO hydroxyl ratios of 30/70 and 50/50, obtained at 25 °C, were reported in a previous study [19] and used for comparison in the present study.

Table 1 presents the codes and formulations used for the resulting films.

Table 1. Codes and formulations.

Codes *	Formulation	Mass Ratio	Synthesis Temperature ** (°C)	Hydroxyl Content from	
				PKL-Glu	CO
$LignoPU_{COPKL30}$_25 ***	CO/PKL30%/pMDI	1.8:0.5:1	25	30	70
$LignoPU_{COPKL30}$_50			50		
$LignoPU_{COPKL30}$_75			75		
$LignoPU_{COPKL30}$_100			100		
$LignoPU_{COPKL50}$_25 ***	CO/PKL50%/pMDI	1.2:0.8:1	25	50	50
$LignoPU_{COPKL50}$_50			50		
$LignoPU_{COPKL50}$_75			75		
$LignoPU_{COPKL50}$_100			100		
$LignoPU_{COPKL\text{-}Glu30}$_25	CO/PKL-Glu30%/pMDI	1.8:0.5:1	25	30	70
$LignoPU_{COPKL\text{-}Glu30}$_50			50		
$LignoPU_{COPKL\text{-}Glu30}$_75			75		
$LignoPU_{COPKL\text{-}Glu30}$_100			100		
$LignoPU_{COPKL\text{-}Glu50}$_25	CO/PKL-Glu50%/pMDI	1.2:0.8:1	25	50	50
$LignoPU_{COPKL\text{-}Glu50}$_50			50		
$LignoPU_{COPKL\text{-}Glu50}$_75			75		
$LignoPU_{COPKL\text{-}Glu50}$_100			100		

* Polymeric methylene diphenyl diisocyanate (pMDI), castor oil (CO), purified Kraft lignin (PKL), purified Kraft lignin hydroxyalkylated (PKL-Glu), LignoPU films using pMDI as isocyanate and PKL-Glu ($LignoPU_{COPKL\text{-}Glu}$). ** Temperature used for the synthesis after spreading the reaction mixtures onto glass plate surfaces for the subsequent formation of films. *** Data for $LignoPU_{COPKL30}$_25 and $LignoPU_{COPKL50}$_25 extracted from [19].

Samples were collected from the reaction mixture immediately after deposition onto the glass plate (at time zero) and then analyzed by Fourier transform infrared spectroscopy (FTIR). Film formation was monitored until the isocyanate band in the spectra was no longer detectable. After the reaction was complete, the films were removed from the plate and stored under vacuum in a silica-containing desiccator.

2.4. Characterizations

2.4.1. PKL-Glu

Figure 3 presents the PKL-Glu analyses. For size-exclusion chromatography (SEC) and ^{1}H nuclear magnetic resonance (NMR) spectroscopy, the samples were first acetylated to minimize macromolecular aggregation in solution.

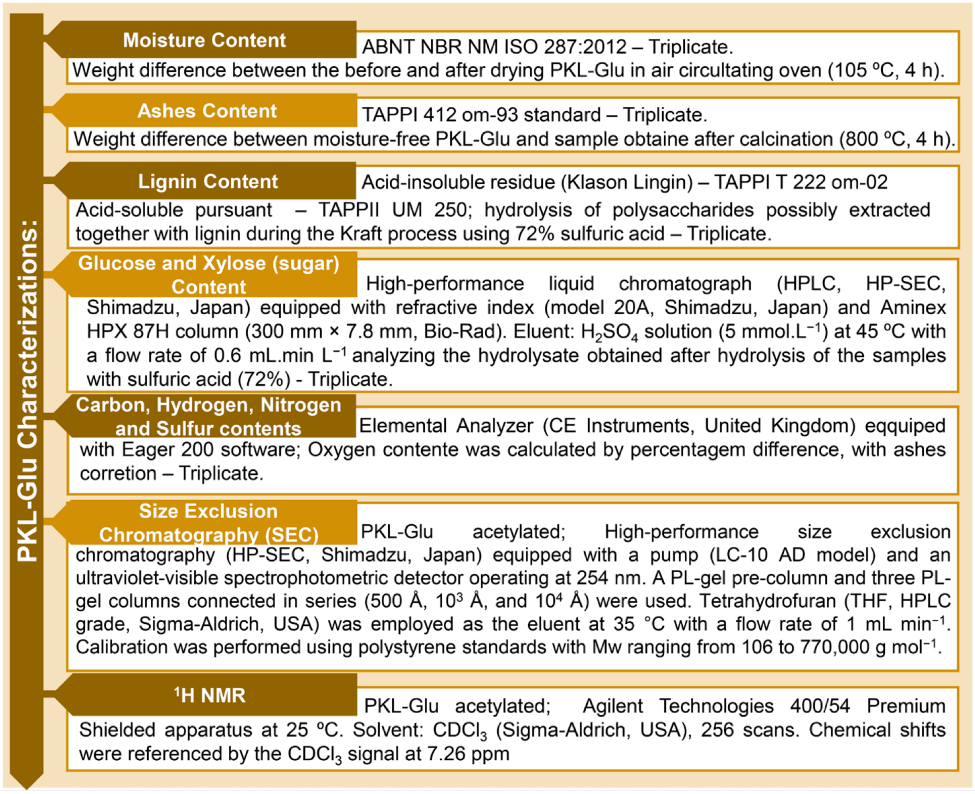


Figure 3. PKL-Glu characterizations.

The samples were acetylated with a pyridine/acetic anhydride mixture (1:1, *v*/*v*) under reflux at 60 °C for 24 h. After the reaction, methanol was added to quench excess acetic anhydride, and the mixture was refluxed for 3 h. Solvents and reaction by-products were then removed by successive evaporation and co-distillation with toluene and methanol. The acetylated material was dried and stored in a silica gel desiccator. FTIR spectroscopy (IRAffinity-1, Shimadzu, Japan) confirmed the acetylation in the 4000–400 cm^{-1} region, using 32 scans and 4 cm^{-1} resolution (spectra not shown). Analyses were performed using KBr pellets prepared from dried spectroscopic-grade KBr and the acetylated materials [19].

2.4.2. LignoPU Films Characterization

Fourier Transform Infrared Spectroscopy (FTIR)

Spectra were recorded using an IRAffinity-1 spectrometer (Shimadzu, Japan) in the 4000–650 cm^{-1} spectral range, with a resolution of 4 cm^{-1} and 32 scans. Measurements for the formed films were carried out in attenuated total reflectance (ATR) mode.

Thermogravimetric Analysis (TGA)

Thermal stability was assessed by thermogravimetric analysis on a Shimadzu TGA-50 (Shimadzu Corporation, Kyoto, Japan). Samples weighing 8 to 9 mg were heated from 25 to 900 °C at 10 °C min^{-1} under a nitrogen atmosphere at 50 mL min^{-1}, using platinum sample holders.

X-Ray Diffraction

The degree of crystallinity of the films was evaluated by X-ray diffraction on a Bruker D8 Advance diffractometer (Bruker AXS GmbH, Karlsruhe, Germany) equipped with a LynxEye detector and DIFFRAC EVA V4 software. Diffraction patterns were recorded at room temperature (approximately 25 °C) under ambient conditions over a 2θ range of 5° to 60°. A step size of 0.02° was used, with a counting time of 0.5 s per step.

Using Bruker's DIFFRAC EVA v7.0 software, after baseline adjustment of the X-ray diffractograms, the total area and peak area were determined. The percentage of non-crystalline regions was calculated as (Total Area − Peak Area)/Total Area. Subtracting this value from 100 yields the CrI (%).

Contact Angles

The wettability of the film surfaces was evaluated using dynamic contact angle measurements at 25 °C with a CAM 200 goniometer (KSV Instruments, Helsinki, Finland) and CAM 2008 image analysis software. A droplet of deionized water (approximately 5 μL) was placed on each film sample, which measured 1.0 ± 0.1 cm by 1.0 ± 0.05 cm. The contact angles on both sides of the droplet were determined from the captured images. Measurements were taken at 1 s intervals, yielding 200 data points per sample.

Dynamic-Mechanical Analysis (DMA)

Dynamic mechanical properties were measured using a Q800 DMA instrument (TA Instruments, New Castle, DE, USA) in tensile mode. Samples measuring 6.4 mm in width, 5.0 mm in gauge length, and 0.65 mm in thickness were tested under the following conditions: an oscillation amplitude of 20 μm, a preload of 0.01 N, a frequency of 1 Hz, and a heating rate of 3 °C/min. The testing temperature range was −100 °C to 230 °C. All measurements were conducted in triplicate.

Tensile Tests

Mechanical properties were assessed at 25 °C utilizing a Q800 DMA analyzer (TA Instruments, New Castle, DE, USA) in tensile mode. Specimens measuring 1.5 mm in gauge length, 5.0 mm in width, and 0.65 mm in thickness were tested. Each test included a force ramp of 1 N/min, reaching a maximum of 18 N, along with an initial preload of 0.001 N. All measurements were conducted in triplicate.

Scanning Electron Microscopy (SEM)

The morphology of the films was analyzed using a Zeiss DSM 940 scanning electron microscope (Carl Zeiss, Oberkochen, Germany) at an accelerating voltage of 20 kV. Prior to analysis, both non-fractured and cryofractured samples were coated with a thin layer of gold by sputter coating using a BAL-TEC metallizer (MED 020, Balzers, Liechtenstein).

3. Results and Discussion

3.1. Purified Kraft Lignin Hydroxyalkylated (PKL-Glu)

The results of the chemical characterization of the modified lignin are presented in Table 2. Data from PKL extracted from [19] are also presented in Table 2. Typically, Kraft-type lignin contains 1–2% sulfur [31]. The residual sulfur in the purified, unmodified Kraft lignin (PKL) was 1.8% [19]. After the glutaraldehyde modification reaction, the sulfur content decreased by 62.6% (Table 2), thereby improving the lignin's characteristics for subsequent application in the synthesis of PUs.

Table 2. PKL-Glu characterization.

Analysis	PKL *	PKL-Glu
Moisture (%)	3.8 ± 0.2	4.3 ± 0.4
Ashes (%)	0.1 ± 0.09	0.1 ± 0.05
Carbon (%)	61.3	62.7
Hydrogen (%)	5.6	7.2
Nitrogen (%)	0.7	0.0
Sulfur (%)	1.8	0.7
Oxygen (%)	30.4	29.2
Glucose (%)	2.700 ± 0.004	ND **
Xylose (%)	2.280 ± 0.002	ND **
Total Sugars (%)	4.980 ± 0.003	ND **
Acid Soluble Lignin (%)	9.0 ± 0.8	9 ± 1
Acid Insoluble Lignin (%)	85.1 ± 1.2	87 ± 3
Total Lignin (%)	94.1 ± 1.4	96 ± 2
Mw (g/mol) ***	2331	4421
Mw/Mn ***	2.0	4.0
Aliphatic OH (mmol/g) ***	0.9	2.4
Aromatic OH (mmol/g) ***	3.2	3.4
Total OH (mmol/g) ***	4.1	5.8

PKL: purified Kraft lignin; PKL-Glu: hydroxyalkylated PKL. * Data extracted from [19]. ** Not detected. *** Acetylated PKL and PKL-Glu.

The average molar mass of acetylated PKL-Glu was 4421 g/mol, with a polydispersity of 4.0, whereas for acetylated PKL, the values were 2331 g/mol and a polydispersity of 2.0 [19]. Given the bifunctionality of glutaraldehyde, the reaction with free positions on lignin's aromatic rings can link two molecules via a bridge (Figure 1), resulting in an increase in the average molar mass [4,32]. This reaction did not engage all lignin molecules present in the medium, resulting in increased dispersity.

Hydroxyalkylation increases the hydroxyl content (Table 2), which constitutes the primary reactive site for isocyanates. The key factor is the average hydroxyl density per lignin unit, which determines overall reactivity. Consequently, the increased dispersity does not inhibit the reaction, as the greater availability of hydroxyl groups may offset this effect.

^{1}H NMR spectroscopy was primarily used to qualitatively and quantitatively assess the aliphatic and aromatic hydroxyl groups in PKL and PKL-Glu after acetylation (Figure 4) [33]. Acetylation enables indirect determination of hydroxyl groups by identifying and integrating signals from the corresponding acetate groups. Table 3 summarizes the possible assignments of the main signals observed in the ^{1}H NMR spectra of acetylated PKL and PKL-Glu.

Table 3. Peaks observed in the ^{1}H NMR spectrum of PKL and PKL-Glu and their possible assignments [33,34].

Chemical Shifts (ppm)	Possible Assignments
6.25–7.90	Aromatic region
5.75–6.25	H α in β-O-4 units and ethylenic protons
5.20–5.80	H α in benzyl aryl ethers
3.55–3.95	Methoxyl groups
2.20–2.50	Region of aromatic acetates
1.60–2.20	Region of aliphatic acetates
<1.60	Non-oxygenated aliphatic region

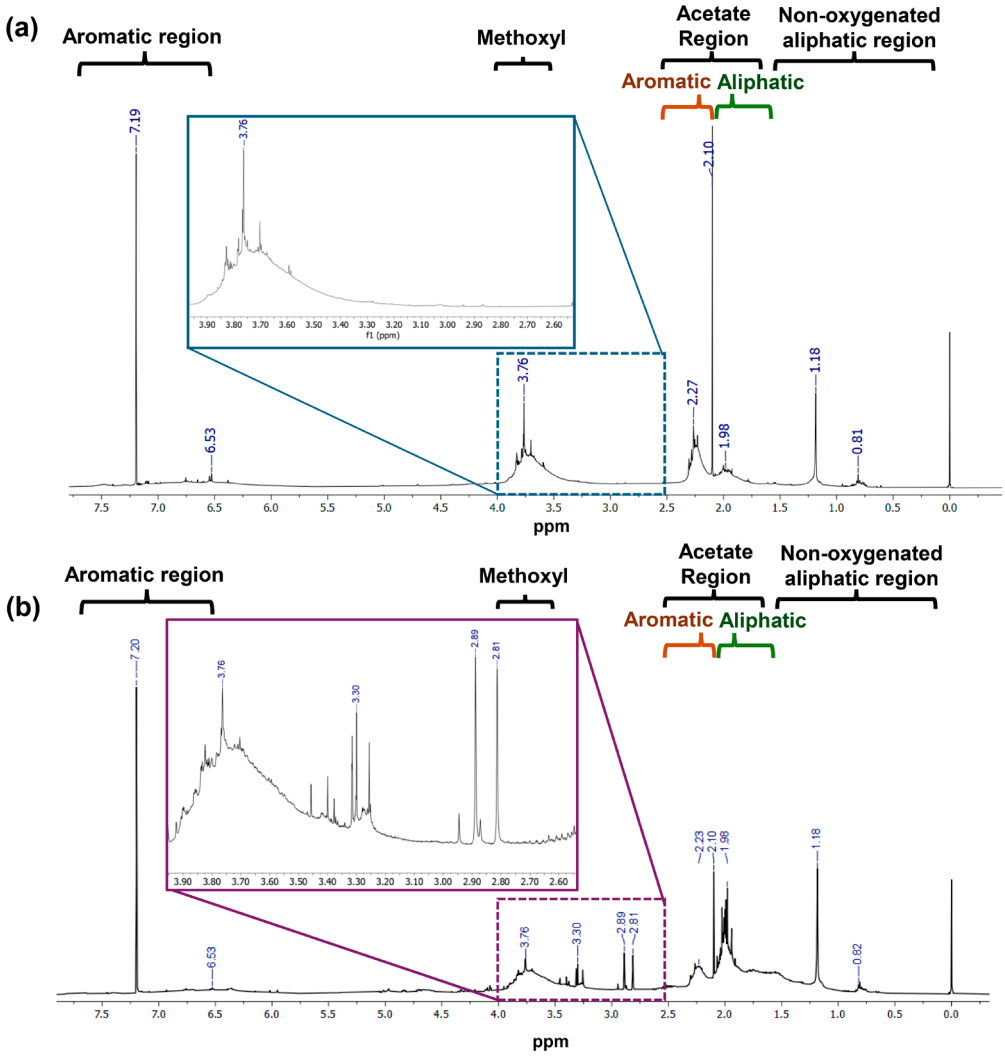


Figure 4. ^{1}H NMR spectrum of acetylated (**a**) PKL and (**b**) PKL-Glu ($CDCl_3$ solvent, 256 scans); magnification of the 2.5 ppm to 4.0 ppm region. Note: Data for PKL were extracted from [19]. Reproduced with permission from Elsevier, order license ID 1785892-1.

The main signals in the spectra of PKL and PKL-Glu fall within similar chemical shift regions, indicating that the characteristic structural features of PKL were preserved after reaction with glutaraldehyde (Figure 4). The signal at approximately 3.76 ppm is assigned to methoxyl groups, whereas the signals in the aromatic region are assigned to protons on lignin's aromatic structures. The region between 5.20 and 6.25 ppm can be assigned to protons in β-O-4 structures, benzyl aryl ethers, and ethylenic structures, according to the assignments presented in Table 3 [33,34].

After acetylation, the signals in the 2.20–2.50 and 1.60–2.20 ppm regions are attributed to aromatic and aliphatic acetates, respectively (Figure 4, Table 3). These signals correspond to hydroxyl groups in the PKL and PKL-Glu structures prior to acetylation, which are converted to acetate groups during the derivatization procedure. Comparison of the spectra in Figure 4 shows that, although the main signals are present in both samples, the aliphatic acetate region is broader and more pronounced for PKL-Glu than for PKL. This difference is consistent with an increased contribution of aliphatic acetate groups after glutaraldehyde treatment, indicating increased aliphatic hydroxyl functionality in the modified lignin.

The aliphatic, aromatic, and total hydroxyl (OH) contents, determined from the ^{1}H NMR spectra by integrating the areas of the aromatic and aliphatic acetate regions, are presented in Table 2. For PKL, the aliphatic, aromatic, and total OH contents were 0.9,

3.2, and 4.1 mmol g^{-1} [19], respectively, whereas PKL-Glu exhibited values of 2.4, 3.4, and 5.8 mmol g^{-1}, respectively. This indicates that the aliphatic OH content increased by approximately 2.7-fold (167%), from 0.9 to 2.4 mmol g^{-1}. In contrast, the aromatic OH content remained largely unchanged, increasing only slightly from 3.2 to 3.4 mmol g^{-1}. Consequently, the increase in total hydroxyl content, from 4.1 to 5.8 mmol g^{-1}, is predominantly due to the rise in aliphatic hydroxyl groups. These measurements were then related to the total integration area of the hydrogen signals in the ^{1}H NMR spectrum and to the C9 formula of PKL-Glu ($C_9H_{13.6}O_{1.18}(OCH_3)_{3.03}$; molar mass = 234.44 g/mol), derived from elemental analysis of PKL-Glu [34].

The higher aliphatic OH content of PKL-Glu is particularly relevant to its use as a polyol in PU synthesis. In this regard, the ^{1}H NMR results, together with the average molar mass analyses, provide evidence that glutaraldehyde treatment altered the hydroxyl functionality of PKL mainly by increasing the availability of aliphatic OH groups while largely preserving the aromatic hydroxyl content.

The 2.5–4.0 ppm region was magnified to highlight the difference between the PKL and PKL-Glu spectra. The observed signals can be attributed to hydrogen atoms in the bridge formed between two lignin molecules following reaction with glutaraldehyde: Lig-CH(OH)-CH_2-CH_2-CH_2-CH(OH)-Lig, which was converted via acetylation into Lig-CH**a**(O-$COCH_3$**b**)-CH_2**c**-CH_2**d**-CH_2**c**-CH**a**(O-$COCH_3$**b**)-Lig. Presumably, H**a** is the most deshielded and H**d** the least deshielded, with H**b** and H**c** having signals located in intermediate positions between H**a** and H**d**. Given that the environment of these H atoms also involves aromatic rings linked to other functional groups, identifying signal multiplicity is somewhat difficult. This difference between the PKL and PKL-Glu spectra, combined with the increase in hydroxyl groups, confirms that the primary reaction involved forming a bridge between lignin molecules.

3.2. LignoPU Films

3.2.1. Infrared Spectroscopy

Infrared spectra were acquired for the reaction mixtures designated LignoPU$_{COPKL30}$, LignoPU$_{COPKL-Glu30}$, LignoPU$_{COPKL50}$, and LignoPU$_{COPKL-Glu50}$. Spectra were recorded immediately after deposition on the plate (at time = 0 h) and for the corresponding films formed from these reaction mixtures at 25 °C, 50 °C, 75 °C, and 100 °C. The spectra for LignoPU$_{COPKL-Glu50}$ are presented in Figure 5, while those for the other mixtures are provided in the Supplementary Information (S.I.), Figures S1–S3.

The infrared region analyzed spans 4000 to 650 cm^{-1}, highlighting key regions with characteristic PU bands. These include:

- 3050–3720 cm^{-1}, corresponding to the N-H stretching vibration,
- 2800–3000 cm^{-1}, related to the C-H stretching vibration,
- 1665–1780 cm^{-1}, associated with the carbonyl (C=O) stretching vibration in urethanes (amide I) [35].

The spectra in Figure 5 and S.I. (Figures S1–S3) indicate that after mixing the reagents and depositing them on the plate (referred to as time 0 h), the isocyanate (NCO) band at 2277–2272 cm^{-1}, sourced from pMDI, was prominent but was no longer detected in the film spectrum. This observation indicates that all the isocyanate reacted with the hydroxyl groups of CO, PKL, or PKL-Glu. Additionally, the band around 3413–3354 cm^{-1} was intense at 0 h, attributed to OH groups from CO, PKL, or PKL-Glu (as shown in Figure 5 and S.I.). However, this band's intensity decreased significantly in the film. This decrease can be attributed to N-H stretching vibrations in the urethane group (-O-CO-NH-) at approximately 3341–3320 cm^{-1}, as well as to aromatic hydroxyl groups in PKL or PKL-Glu, which are less reactive than their aliphatic counterparts.

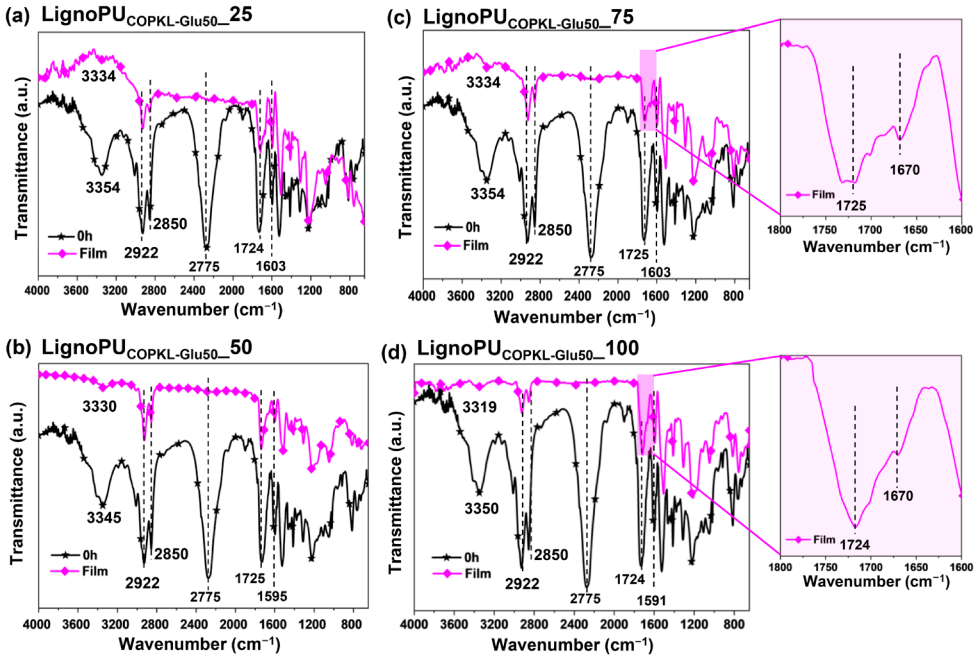


Figure 5. FTIR spectra of the reaction mixtures (CO, PKL-Glu50%, and pMDI) in the region of 4000 to 650 cm^{-1}, immediately after deposition on the plate, and of the LignoPU$_{COPKL-Glu50}$ films formed at temperatures of (**a**) 25 °C, (**b**) 50 °C, (**c**) 75 °C, and (**d**) 100 °C. Magnification of the 1600–1800 cm^{-1} region in (**c**,**d**).

The carbonyl band in PUs (1650–1740 cm^{-1}) indicates carbonyl (C=O) groups linked to N-H groups that are either involved in hydrogen bonds or are free (Figure 5).

Allophanate groups can form via a secondary reaction that may proceed slowly at 60 °C and accelerate significantly at 100 °C and above. Literature indicates that the carbonyl vibration of the NH-bonded carbonyl in allophanates appears as a shoulder on the urethane carbonyl band. The position of this shoulder varies across reports, with citations placing it around 1650 cm^{-1} or lower [36,37] or in the 1685 cm^{-1} region [38], among others. In the present study, we observe a subtle shoulder at 1670 cm^{-1} in the LignoPU$_{COPKL50}$ (Figure S3) and in LignoPU$_{COPKL-Glu50}$ films formed at 75 °C (Figure 5c) and 100 °C (Figure 5d). This feature could tentatively be attributed to allophanate-type groups in PUs synthesized from 50% PKL or PKL-Glu at temperatures above 60 °C. It can be hypothesized that the 50 CO/50 PKL (or PKL-Glu) ratio established a balance between flexibility (from ricinoleic acid triglyceride, CO) and rigidity (from PKL or PKL-Glu). This balance enhanced the mobility and accessibility of the urethane groups formed during synthesis, allowing them to react further with an isocyanate group to generate allophanate groups. This process occurred only to a limited extent, as shown by the shoulder's intensity up to 1670 cm^{-1}.

3.2.2. Thermogravimetric Analysis

The thermal decomposition of PUs typically occurs in two or three stages, and the composition of the resulting decomposition products is influenced by PU structure [39]. TG (Figure S4) and dTG profiles (Figure S5) revealed differences based on lignin content. Films obtained from 30% PKL or PKL-Glu exhibited three decomposition events (Table 4), whereas those obtained from 50% PKL or PKL-Glu showed only two main events (Table 5). In addition, the latter displayed higher residual masses at 900 °C (approximately 20–26%) than the corresponding films obtained from 30% PKL (approximately 11–17%). These results are consistent with the higher content of aromatic structures introduced by lignin, which favors char formation during thermal decomposition.

Table 4. Temperatures of the thermal events and residual mass of the $LignoPU_{COPKL30}$ and $LignoPU_{COPKL\text{-}Glu30}$ films formed during reactions at 25, 50, 75, and 100 °C.

Film	1st Event (300–360 °C)		2nd Event (360–415 °C)	3rd Event (415–565 °C)	Residue (900 °C)
	T_{onset} (°C)	$T_{Máx}$ (°C)	$T_{Máx}$ (°C)	$T_{Máx}$(°C)	Mass (%)
$LignoPU_{COPKL30}$_25 *	315	343	380	468	16.4
$LignoPU_{COPKL30}$_50	311	341	376	481	13.6
$LignoPU_{COPKL30}$_75	315	350	376	469	16.8
$LignoPU_{COPKL30}$_100	312	345	377	473	16.4
$LignoPU_{COPKL\text{-}Glu30}$_25	309	346	380	480	10.9
$LignoPU_{COPKL\text{-}Glu30}$_50	310	346	382	476	12.8
$LignoPU_{COPKL\text{-}Glu30}$_75	315	347	379	482	14.8
$LignoPU_{COPKL\text{-}Glu30}$_100	309	346	377	480	15.4

LignoPU: lignopolyurethane; CO: castor oil; PKL: purified Kraft lignin; PKL-Glu: hydroxyalkylated PKL; T_{onset}: initial decomposition temperature; $T_{Máx}$: maximum mass loss rate temperature. * Data for $LignoPU_{COPKL30}$_25 extracted from [19].

Table 5. Temperatures of the thermal events and residual mass of the $LignoPU_{COPKL50}$ and $LignoPU_{COPKL\text{-}Glu50}$ films formed during reactions at 25, 50, 75, and 100 °C.

Film	1st Event (300–400 °C)		2nd Event (400–565 °C)	Residue (900 °C)
	T_{onset} (°C)	$T_{Máx}$ (°C)	$T_{Máx}$(°C)	Mass (%)
$LignoPU_{COPKL50}$_25 *	316	363	473	24.7
$LignoPU_{COPKL50}$_50	311	363	475	23.0
$LignoPU_{COPKL50}$_75	312	369	478	22.7
$LignoPU_{COPKL50}$_100	310	362	472	25.9
$LignoPU_{COPKL\text{-}Glu50}$_25	302	354	476	20.7
$LignoPU_{COPKL\text{-}Glu50}$_50	305	363	477	19.5
$LignoPU_{COPKL\text{-}Glu50}$_75	306	345	462	22.8
$LignoPU_{COPKL\text{-}Glu50}$_100	310	358	453	26.0

LignoPU: lignopolyurethane; CO: castor oil; PKL: purified Kraft lignin; PKL-Glu: hydroxyalkylated PKL; T_{onset}: initial decomposition temperature; $T_{Máx}$: maximum mass loss rate temperature. * Data for $LignoPU_{COPKL50}$_25 extracted from [19].

dTG curves (Figure S5) showed that the first event, associated with the breakdown of urethane bonds of the type (-HN-CO-O-) and the release of CO, CO_2, amines, and aldehydes [40,41], had maximum mass loss rate temperatures (TMáx) between 341 °C and 350 °C for films containing 30% PKL or 30% PKL-Glu, regardless of the synthesis temperature. For films containing 50% PKL or PKL-Glu, higher TMáx values were observed, ranging from 354 °C to 363 °C for $LignoPU_{COPKL\text{-}Glu50}$ and from 362 °C to 369 °C for $LignoPU_{COPKL50}$. In addition to urethane group decomposition, this temperature range, which partially overlaps with that of films formed from reactions using 30% and 50% PKL or PKL-Glu, may also be associated with the onset of decomposition of flexible segments originating mainly from the ricinoleic acid triglyceride chains (from CO).

The final event occurred within a temperature range of 400 to 565 °C across all examined materials (Tables 4 and 5). This event involves the cleavage of various bonds, including C-C, C-O, C-H, C=C, and C=O [42]. It is primarily associated with the decomposition of more thermally stable structures. Higher decomposition temperatures indicate more organized regions within the materials, arising from stronger intermolecular interactions that require more energy to decompose [43].

The films exhibited thermal stability up to approximately 300 °C (Initial decomposition temperature, T_{onset}, Tables 4 and 5). Furthermore, no significant mass loss was observed

below 100 °C, indicating low moisture content in the materials. The thermal stability of PUs is related to the presence of rigid segments (aromatic rings of pMDI and of PKL or PKL-Glu) and flexible segments introduced by the ricinoleic acid triglyceride chains (from CO) in their chemical structure, as well as the molar ratio between the two [44]. The T_{onset} values (Tables 4 and 5) remained essentially unchanged as the synthesis temperature increased. Likewise, the TG (Figure S4) and dTG (Figure S5) curves showed very similar thermal decomposition profiles across all films.

3.2.3. X-Ray Diffraction

X-ray diffraction (Figure 6) was used to evaluate the crystallinity of films formed during syntheses using PKL or PKL-Glu at 30% and 50% relative to CO, as well as pMDI, at temperatures of 25, 50, 75, and 100 °C.

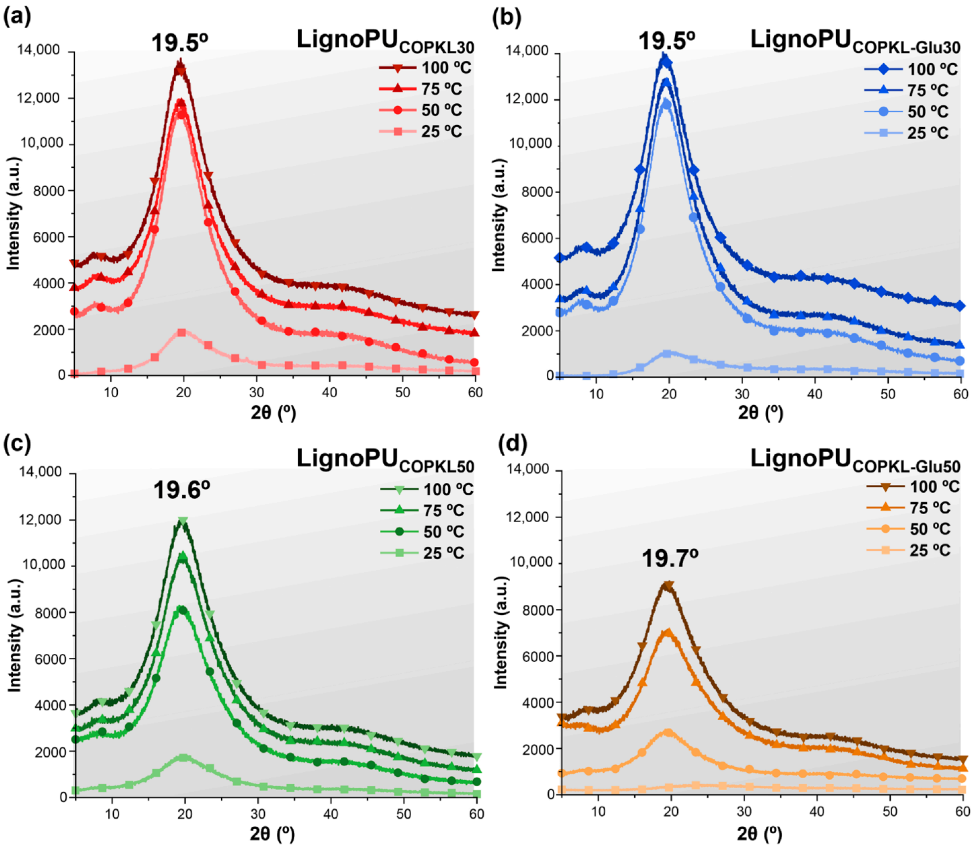


Figure 6. X-ray diffractograms for films produced at 25 °C, 50 °C, 75 °C and 100 °C: (**a**) $LignoPU_{COPKL30}$ (**b**) $LignoPU_{COPKL-Glu30}$, (**c**) $LignoPU_{COPKL50}$ e (**d**) $LignoPU_{COPKL-Glu50}$. Note:The diffractogram baselines were offset to improve visualization. Data for $LignoPU_{COPKL30}$_25 and $LignoPU_{COPKL50}$_25 were extracted from [19].

In all films produced, an intense peak appeared at approximately 2θ = 19.5–19.7° (Figure 6), indicating the formation of ordered regions in the films. These angles are close to those observed in films produced by synthesizing PUs from castor oil-derived polyesters and MDI at different NCO/OH ratios (2θ = 19°) [45].

The peak at 2θ = 19.5–19.7° (Figure 6) can be attributed to short-range order, typically arising from rigid segments [46] with urethane groups involved in hydrogen bonding. Given the non-linear structure of the KL used as a polyol (PKL and PKL-Glu), it is assumed that the rigid structures typical of pMDI, linked to flexible segments originating from ricinoleic acid triglyceride (from CO), may have primarily contributed to the formation of the crystalline regions.

The X-ray diffraction curves (Figure 6) and Table 6 show a marked difference in the crystallinity index (CrI) between films formed at 25 °C and those formed above room temperature. The CrI values were calculated from the area under the peak and the total area of the diffractogram, as described in the experimental section; therefore, they do not depend solely on peak intensity.

Table 6. CrI of LignoPU$_{COPKL30}$, LignoPU$_{COPKL\text{-}Glu30}$, LignoPU$_{COPKL50}$, and LignoPU$_{COPKL\text{-}Glu50}$ films formed during synthesis at 25 °C, 50 °C, 75 °C, and 100 °C.

Film	CrI (%)			
	25 °C	**50 °C**	**75 °C**	**100 °C**
LignoPU$_{COPKL30}$	36 *	62	61	61
LignoPU$_{COPKL\text{-}Glu30}$	28	64	63	62
LignoPU$_{COPKL50}$	35 *	55	55	58
LignoPU$_{COPKL\text{-}Glu50}$	13	43	58	54

LignoPU: lignopolyurethane; CO: castor oil; PKL: purified Kraft lignin; PKL-Glu: hydroxyalkylated PKL; CrI: crystallinity index. * Data for LignoPU$_{COPKL30}$_25 and LignoPU$_{COPKL50}$_25 extracted from [19].

Replacing PKL with PKL-Glu as the polyol produced films with lower CrI values when the film-forming reaction was carried out at 25 °C (LignoPU$_{COPKL\text{-}Glu50}$_25, CrI = 13%) or 50 °C (LignoPU$_{COPKL\text{-}Glu50}$_50, CrI = 43%) using 50% PKL-Glu (Table 6). This likely occurred because the PKL-Glu macromonomer has an average molar mass of 4421 g/mol, whereas PKL has an average molar mass of 2331 g/mol (Table 2). The higher average molar mass and greater structural complexity of the PKL-Glu macromonomer are reflected in the chemical structure of the resulting PU film; under the specified reaction conditions, the organization of segments capable of forming crystalline regions was likely more difficult for LignoPU$_{COPKL\text{-}Glu50}$_25 and LignoPU$_{COPKL\text{-}Glu50}$_50 than for LignoPU$_{COPKL_50}$_25 and LignoPU$_{COPKL}$_50, leading to the observed results.

Higher temperatures greatly accelerate the reaction rate, enabling faster network and film formation. One possibility is that although higher temperatures favor segment mobility and organization, the structure that forms more rapidly may limit the formation of more crystalline domains. Crystallinity practically does not advance beyond that achieved in the film formed during the reaction at 50 °C. It can also be conjectured that the reaction occurring on a glass surface, with PU production and film structuring restricted to a thickness of 0.5 mm, may lead to confinement that also helps prevent the formation of additional crystalline regions.

LignoPUCO$_{PKL\text{-}Glu50}$ exhibits distinct behavior: film crystallinity increases as the reaction temperature rises from 50 °C to 75 °C, but remains nearly unchanged at 100 °C. Notably, the film produced at 50 °C has not yet reached its crystallization limit for this formulation, indicating that additional crystalline regions may still form.

3.2.4. Contact Angle

The initial and final contact angles (CA) between the film surface and the water droplet deposited on it are shown in Figure 7. The final contact angle was recorded after 200 s of observation.

The initial CA values for the LignoPU$_{COPKL30}$ and LignoPU$_{COPKL50}$ films synthesized at room temperature were 82 ± 1° and 80 ± 1°, respectively [19], whereas the LignoPU$_{COPKL\text{-}Glu30}$ and LignoPU$_{COPKL\text{-}Glu50}$ films prepared under the same conditions showed values of 85 ± 1° and 79 ± 1°, respectively (Figure 7). In general, films synthesized above room temperature exhibited initial CA values close to 100°, higher than those observed for materials obtained at 25 °C, indicating more hydrophobic surfaces. This

behavior suggests a higher proportion of hydrophobic domains oriented toward the film surface at higher synthesis temperatures.

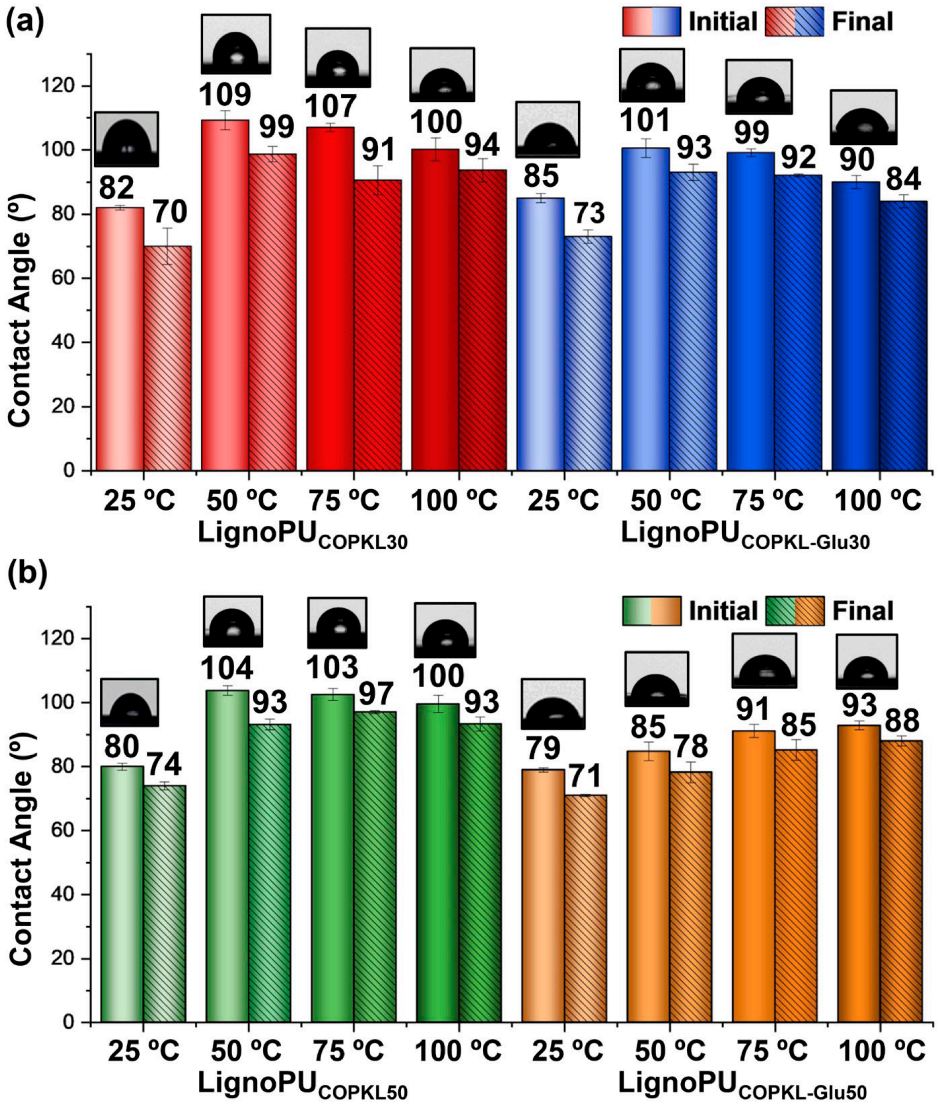


Figure 7. CA initial and final for (**a**) LignoPU$_{COPKL30}$ and LignoPU$_{COPKL-Glu30}$ films and (**b**) LignoPU$_{COPKL50}$ and LignoPU$_{COPKL-Glu50}$ films, and snapshots for the initial contact between the droplet and the surface of the film. Note: Data for LignoPU$_{COPKL30}$_25 and LignoPU$_{COPKL50}$_25 were extracted from [19].

Films prepared at 50 °C exhibited hysteresis of 10°, 8°, 11°, and 7° for LignoPU$_{COPKL30}$, LignoPU$_{COPKL-Glu30}$, LignoPU$_{COPKL50}$, and LignoPU$_{COPKL-Glu50}$, respectively, whereas those synthesized at 100 °C showed 6°, 6°, 7°, and 5°. The decrease in hysteresis with increasing synthesis temperature indicates the formation of films with more homogeneous surfaces.

3.2.5. Dynamic-Mechanical Analysis

Figure 8 shows the Tan δ versus temperature curves for films formed from PUs synthesized with 30% and 50% PKL (LignoPU$_{COPKL30}$ and LignoPU$_{COPKL50}$) and PKL-Glu (LignoPU$_{COPKL-Glu30}$ and LignoPU$_{COPKL-Glu50}$) at temperatures of 25, 50, 75, and 100 °C. The thermal decomposition of the films considered begins above 300 °C (Table 4), which is outside the temperature range considered for DMA.

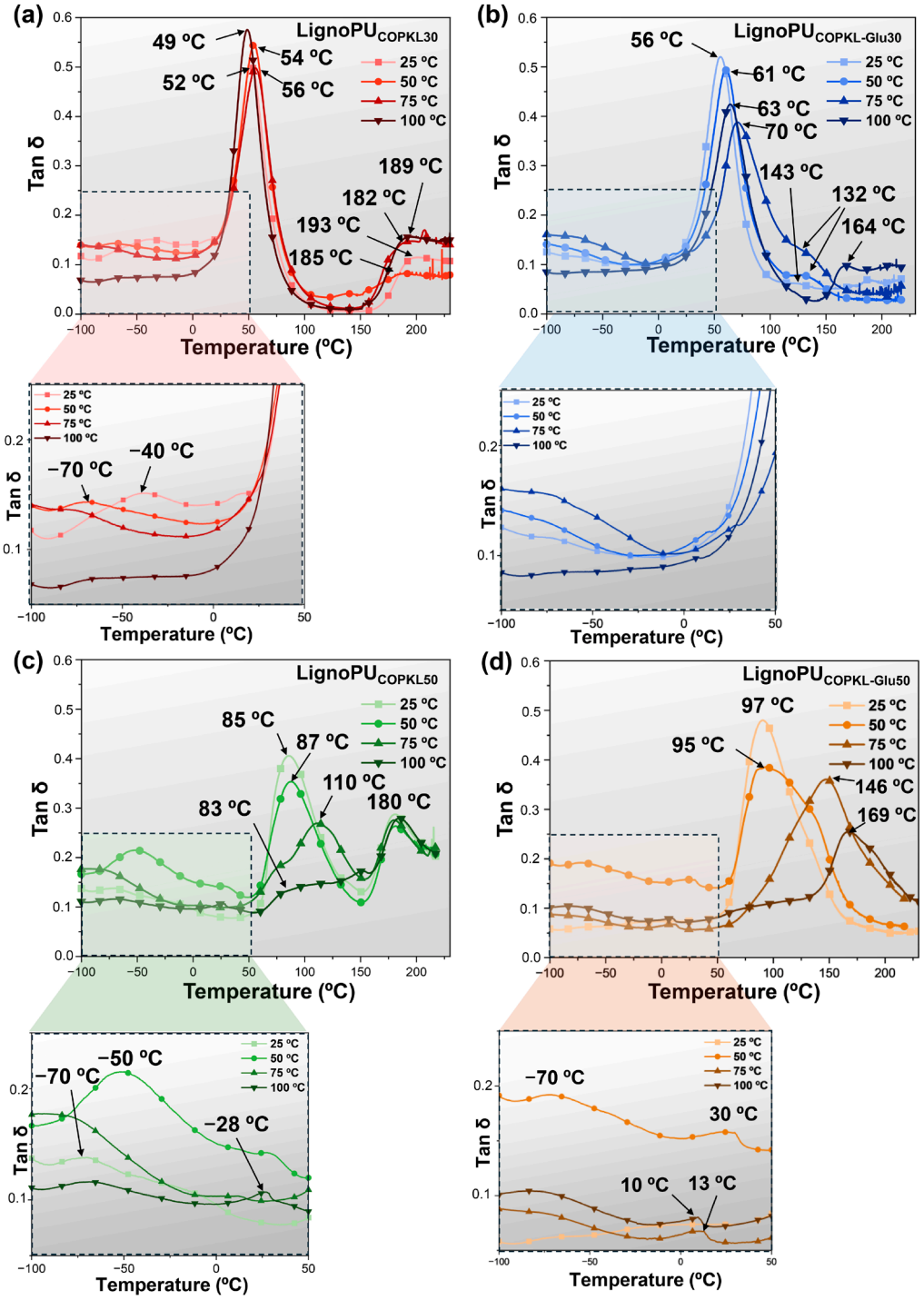


Figure 8. Tan-δ curves for the series (**a**) LignoPU$_{COPKL30}$, (**b**) LignoPU$_{COPKL-Glu30}$, (**c**) LignoPU$_{COPKL50}$ and (**d**) LignoPU$_{COPKL-Glu50}$ at 25, 50, 75 e 100 °C. Note:Data for LignoPU$_{COPKL30}$_25 and LignoPU$_{COPKL50}$_25 were extracted from [19].

The glass transition is related to the mobility of segments within the chemical structure of macromolecules, arising from the rotation of single bonds between atoms that make up these segments. If crystalline domains are present, the glass transition occurs in the non-crystalline domains; the peak temperature of Tan δ can be considered the glass transition temperature (Tg). Depending on the chemical structure of the PUs, flexible domains—where segment mobility is favored- and rigid domains, where mobility is restricted, may exist; in some cases, Tgs for both the flexible and rigid domains can be observed, both of which are present in the non-crystalline regions. Tg is lower in soft

(flexible) domains than in hard (rigid) domains because rotation around single bonds in soft domains requires less energy.

In the present study, the flexible domains can be attributed to the use of ricinoleic acid triglyceride (CO) as a reactant, which has a linear structure (Figure 2), in contrast to the more rigid pMDI. The rigid domains arise from the aromatic ring-rich structures of PKL or PKL-Glu (Figure 2).

For the LignoPU$_{COPKL30}$ series films, increasing the synthesis temperature did not significantly alter the Tan δ curve profile (Figure 8a) or the Tg of the soft segments (49–56 °C). Similarly, the Tg values of the hard segments (182–189 °C) showed no notable changes. This suggests that the chemical structures of the soft and hard regions within the non-crystalline domains remained similar across all temperatures.

The LignoPU$_{COPKL-Glu30}$ series films (Figure 8b) showed changes in their Tan δ curves as the synthesis temperature increased. The film synthesized at 75 °C displayed a broad peak centered at approximately 70 °C, attributed to the Tg of the soft domains, and a shoulder around 132 °C, attributed to the Tg of the hard domains. This indicates that the onset of the glass transition in the hard domains partially overlaps with the glass transition region of the soft domains, suggesting a higher degree of alternation between hard and soft domains within the non-crystalline phase. Conversely, the film formed at 100 °C showed two distinct transitions, indicating greater segregation between the soft and hard phases. This behavior may relate to the higher average molar mass of the PKL-Glu macromonomer compared to PKL, since each PKL-Glu that reacted with pMDI occupied about twice the space in the chemical structure as PKL reacting with pMDI. The higher temperature may have favored reaction sequences --PKL-Glu-pMDI-PKL-Glu--, leading to more extensive rigid segments when PKL-Glu was used as a reagent.

Table 7 presents the Tg values corresponding to the Tan δ peaks for the films in the LignoPU$_{COPKL30}$, LignoPU$_{COPKL50}$, LignoPU$_{COPKL-Glu30}$, and LignoPU$_{COPKL-Glu50}$ series.

Table 7. Tgs (Tan δ peak) for the films in the LignoPU$_{COPKL30}$, LignoPU$_{COPKL50}$, LignoPU$_{COPKL-Glu30}$, and LignoPU$_{COPKL-Glu50}$ series.

PKL Films	T_g (°C)		PKL-Glu Films	T_g (°C)	
	1st Peak	2nd Peak		1st Peak	2nd Peak
LignoPU$_{COPKL30}$_25 *	52	193	LignoPU$_{COPKL-Glu30}$_25	56	143
LignoPU$_{COPKL30}$_50	54	185	LignoPU$_{COPKL-Glu30}$_50	61	132
LignoPU$_{COPKL30}$_75	56	182	LignoPU$_{COPKL-Glu30}$_75	70	132
LignoPU$_{COPKL30}$_100	49	189	LignoPU$_{COPKL-Glu30}$_100	63	164
LignoPU$_{COPKL50}$_25 *	96	193	LignoPU$_{COPKL-Glu50}$_25	87	ND **
LignoPU$_{COPKL50}$_50	89	179	LignoPU$_{COPKL-Glu50}$_50	95	ND
LignoPU$_{COPKL50}$_75	110	179	LignoPU$_{COPKL-Glu50}$_75	146	ND
LignoPU$_{COPKL50}$_100	83	187	LignoPU$_{COPKL-Glu50}$_100	169	ND

LignoPU: lignopolyurethane; CO: castor oil; PKL: purified Kraft lignin; PKL-Glu: hydroxyalkylated PKL; Tg: glass transition temperature; ND: not detected. * Data for LignoPU$_{COPKL30}$_25 and LignoPU$_{COPKL50}$_25 extracted from [19]. ** Not Detected.

For films formed from 50% PKL, increasing the synthesis temperature decreased the intensity and broadened the first relaxation peak, particularly in films obtained at 75 °C and 100 °C. This result indicates fewer flexible segments relaxing and greater structural heterogeneity among the segments involved in the relaxation. In contrast, LignoPU$_{COPKL-Glu50}$ films showed only a single broad peak across all evaluated temperatures, indicating greater mixing between the rigid and flexible phases. Furthermore, increasing the synthesis temperature shifted the Tg values of the formed films to higher temperatures, from 97 °C in

the film obtained at 25 °C to 169 °C in the film obtained at 100 °C. Despite this increase, peak intensity decreased in films prepared at 75 and 100 °C, suggesting fewer rigid and flexible segments in the non-crystalline phase of these materials.

Partially replacing ricinoleic acid triglyceride-derived structures with aromatic structures typical of lignin restricts polymer chain-segment mobility, thereby contributing to the formation of more rigid materials. Thus, increasing the lignin content from 30% to 50% shifts the Tg of the flexible phase to higher temperatures, indicating greater restriction of segment mobility.

Figure 9 shows the storage modulus (E′) at 25 °C for films formed at 25 °C, 50 °C, 75 °C, and 100 °C.

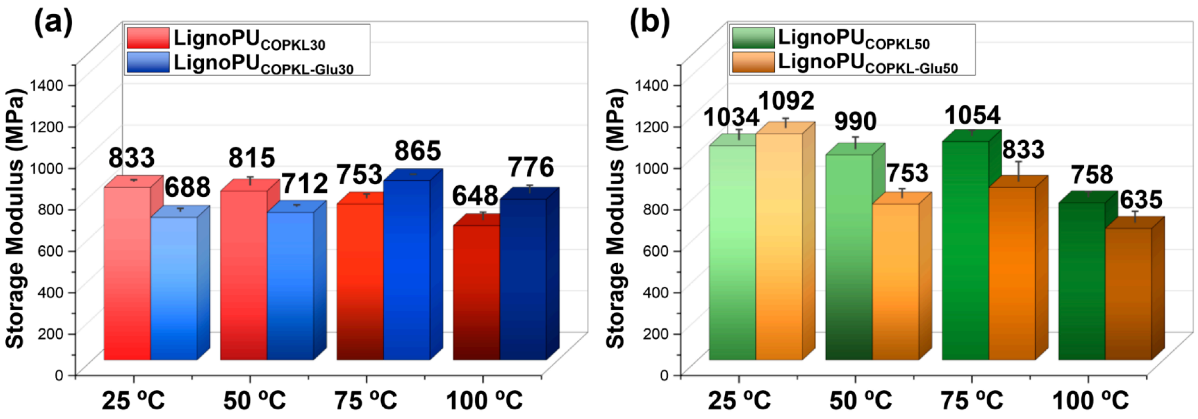


Figure 9. Storage Modulus (E′) at 25 °C of films formed simultaneously with syntheses carried out from (**a**) 30% KL and KL-Glu and (**b**) 50% KL and KL-Glu at temperatures of 25 °C, 50 °C, 75 °C, and 100 °C. Note: Data for LignoPU$_{COPKL30}$_25 and LignoPU$_{COPKL50}$_25 were extracted from [19].

At room temperature (25 °C), where the E′ values are presented (Figure 9), all films formed at temperatures of 25 °C, 50 °C, 75 °C, and 100 °C were in the rigid state because the Tg values observed for these films are above 25 °C (Table 7).

Figure 9 shows that, in general, the increase in temperature during the synthesis of PUs made from 30% LK or LK-Glu did not significantly affect the E′ values of the films, since the E′ values of the films formed at the highest temperatures remained at the level of the films formed at room temperature (LignoPU$_{COPKL30}$_25 = 833 MPa, [19]; LignoPU$_{COPKL-Glu30}$_25 = 688 MPa).

Despite the higher crystallinity (Table 6) of the LignoPU$_{COPKL30}$ and LignoPU$_{COPKL-Glu30}$ films formed at 50 °C, 75 °C, and 100 °C (LignoPU$_{COPKL30}$_50 = 62%; LignoPU$_{COPKL-Glu30}$_50 = 64%; LignoPU$_{COPKL30}$_75 = 61%; LignoPU$_{COPKL-Glu30}$_75 = 63%; LignoPU$_{COPKL30}$_100 = 61%; LignoPU$_{COPKL-Glu30}$_100 = 62%) compared to those formed at 25 °C (LignoPU$_{COPKL30}$_25 = 36%; LignoPU$_{COPKL-Glu30}$_25 = 28%), no significant increase in E′ was observed, indicating that crystallinity did not affect this property at 25 °C, likely because these films were below the Tg at this temperature.

3.2.6. Tensile Properties

Figure 10 presents the results of tensile strength at break, Young's modulus, and elongation at break of LignoPU films formed from 30% and 50% PKL and PKL-Glu at temperatures of 25 °C, 50 °C, 75 °C, and 100 °C.

Tensile tests were conducted at 25 °C. At this temperature, the films formed simultaneously with syntheses performed at 30% and 50% PKL or PKL-Glu, conducted at temperatures of 25 °C, 50 °C, 75 °C, and 100 °C, were in the rigid state, since the Tg values observed for these films are above 25 °C (Table 7).

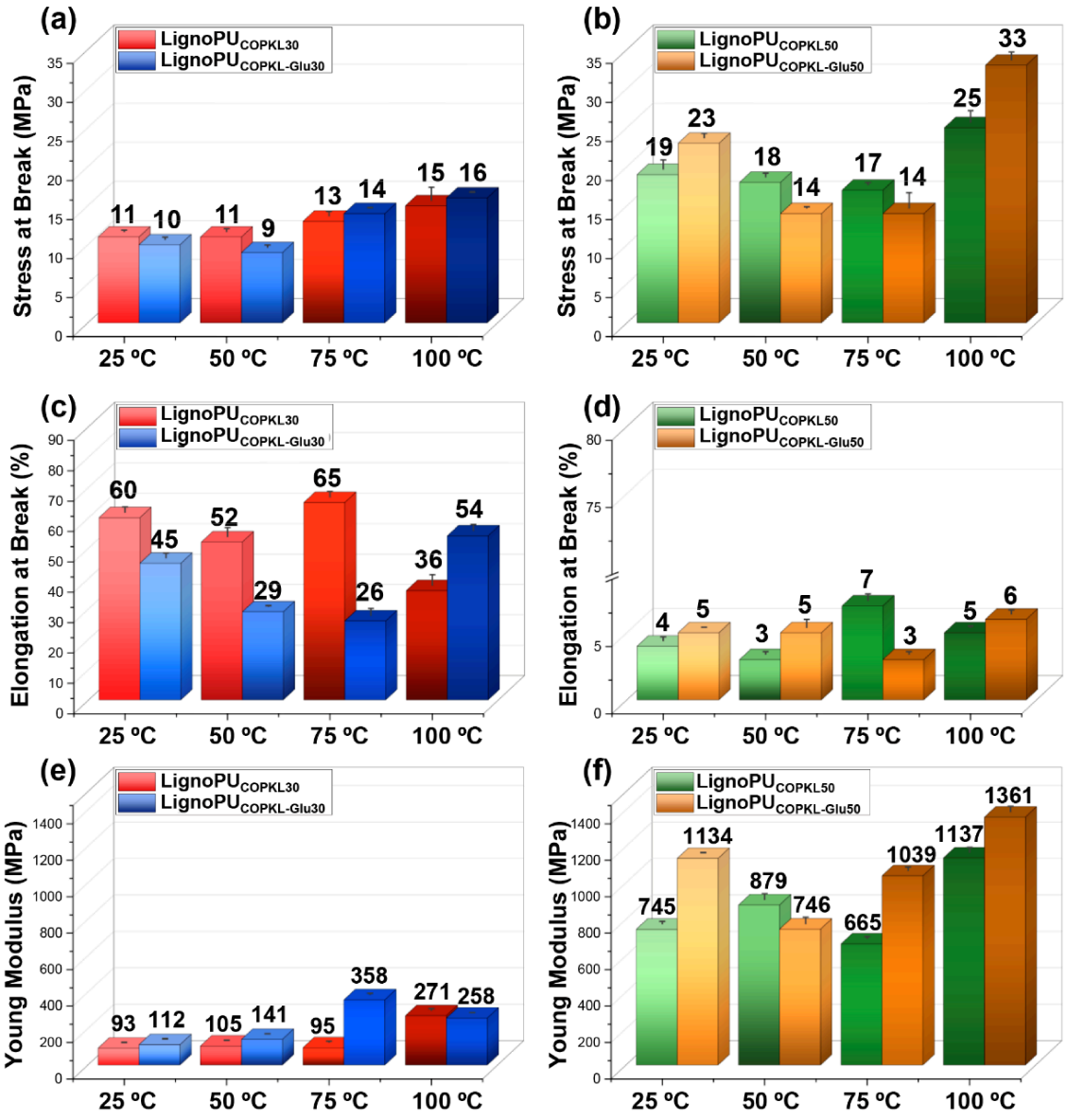


Figure 10. (**a**,**b**) Tensile strength at break, (**c**,**d**) elongation at break, and (**e**,**f**) Young's modulus of films formed simultaneously with the synthesis performed respectively from 30% PKL or PKL-Glu (**a**,**c**,**e**) and 50% PKL or PKL-Glu (**b**,**d**,**f**), at temperatures of 25 °C, 50 °C, 75 °C, and 100 °C. Note: Data for LignoPU$_{COPKL30}$_25 and LignoPU$_{COPKL50}$_25 were extracted from [19].

For the films formed from 30% PKL or PKL-Glu (Figure 10a), the tensile strength at break did not differ significantly between them. However, tensile strength trended upward as the synthesis temperature increased. This may be partly attributed to the higher crystallinity of films produced at temperatures above 25 °C (Table 6). With the exception of the film formed during synthesis at 100 °C, the Young's modulus of the LignoPU$_{COPKL-Glu30}$ series was higher than that of the LignoPU$_{COPKL30}$ series (Figure 10e). This difference likely stems from stronger intermolecular interactions in the LignoPU$_{COPKL-Glu30}$ series. As a result of the increased resistance to deformation, the elongation at break of the LignoPU$_{COPKL-Glu30}$ series was lower compared to that of the LignoPU$_{COPKL30}$ series (Figure 10c). The films formed at 50, 75, and 100 °C have approximately the same crystallinity (Table 6) but show a tendency toward increased tensile strength and a significant increase in Young's modulus. As discussed in Section 3.2.3, the crystallinity of the films reaches a plateau for reactions carried out at 50 °C because, when networks with a higher density of bonds begin to form, these networks prevent further advancement in crystalline-

region formation. The material's mechanical properties are then predominantly influenced by the density of covalent bonds in the networks, which may also involve a higher density of hydrogen bonds, thus increasing the cohesive energy density. As the temperature increases from 50 to 75 and 100 °C, denser networks of covalent and hydrogen bonds can form, mainly increasing resistance to deformation, i.e., Young's modulus.

Films formed from 50% PKL or PKL-Glu exhibited higher tensile strength at break (Figure 10b), considerably higher Young's modulus (Figure 10f), and considerably lower elongation (Figure 10d) than those formed from 30% PKL or PKL-Glu. This results from the higher content of aromatic rings, derived from non-linear structures, in the LignoPKL$_{COPKL50}$ and LignoPU$_{COPKL\text{-}Glu50}$ series, which gives these series considerably superior stiffness. Films formed in syntheses carried out up to 75 °C showed no significant differences in tensile strength at break. Films formed in syntheses carried out at 100 °C exhibited the highest tensile strengths (25 MPa and 33 MPa) and the highest Young's moduli (1137 MPa and 1361 MPa) for LignoPKL$_{COPKL50}$-100 and LignoPKL$_{COPKL\text{-}Glu50}$-100, respectively. The lower proportion of flexible segments in the non-crystalline domains of these films, as indicated by the tanδ curves (Figure 8), may have influenced these results.

Xie et al. (2026) [13] produced PU films from chemically modified castor oil and lignin succinylated with succinic acid, which were then reacted with hexamethylene diisocyanate. They prepared the materials via a solvent-based casting method. The formulation with the highest bio-based content also showed the best mechanical strength, achieving a tensile strength of 10.7 ± 0.9 MPa and an elongation at break of 34 ± 1%. These values are comparable to those observed in the current study for films containing 30 wt% of PKL or PKL-Glu, which ranged from approximately 9 to 16 MPa, but are lower than those for films containing 50 wt% of PKL or PKL-Glu, which ranged from approximately 14 to 33 MPa. The elongation at break values reported by Xie et al. were also similar to those obtained for some films developed in this study. However, Xie et al. (2026) used a diisocyanate that typically imparts greater flexibility to PU than the pMDI used in this study [13]. The authors produced the films from a PU solution, whereas in the present study, the films formed as the reaction progressed without solvent.

Chen et al. (2021) [22] prepared lignin-based PU films from alkaline lignin, polyethylene glycol (PEG-6000), and hexamethylene diisocyanate via solvent casting. The film containing 60 wt% lignin, prepared in tetrahydrofuran at an NCO/OH ratio of 1:1, exhibited a tensile strength of 13.3 MPa, lower than that of the films containing 50 wt% PKL or PKL-Glu in the present work (approximately 14–33 MPa). Moreover, Chen et al. (2021) [22] reported a Young's modulus of 121.6 MPa, substantially lower than the values obtained for the corresponding lignin-rich films in this study, with the lowest values at approximately 665 MPa. Conversely, the elongation at break reported by Chen et al. (2021) [22] reached 465.5%, considerably higher than the values observed in the present work (approximately 5%). This difference may be attributed to the presence of PEG-6000, which acts as a flexible polyol segment and promotes chain mobility, and to the use of hexamethylene diisocyanate instead of the pMDI used in the present study, a source of isocyanate groups bound to aromatic rings that adds rigidity to the material. As Xie et al. (2026) [13] did, the authors produced the films from a PU solution; in contrast, the current study formed the films as the reaction progressed, without a solvent.

Porto et al. (2022) [41] prepared bio-based PU films using microcrystalline cellulose (MCC) and castor oil as polyols and pMDI as the isocyanate source, following a methodology similar to that used in the present work. Films prepared at room temperature with 30 and 50 wt% MCC exhibited tensile strengths of approximately 2.0 MPa and 46 MPa and elongations at break of 46% and 53%, respectively. Although the MCC-containing films showed substantially higher elongation at break, their tensile strengths were lower

than those of the corresponding PKL- and PKL-Glu-containing films developed in this study. The Young's modulus values reported for films containing 30 and 50 wt% MCC were approximately 8 and 77 MPa, respectively, whereas films containing comparable proportions of PKL or PKL-Glu showed values above approximately 90 and 700 MPa. These results indicate that replacing MCC with lignin yields a substantially stiffer PU network, increasing both stiffness and tensile strength at the expense of extensibility. This behavior likely stems from lignin's aromatic, rigid structure and its ability to form strong intermolecular interactions within the PU network.

Overall, these comparisons show that incorporating PKL and PKL-Glu enables the production of bio-based polyurethane films with competitive mechanical strength and substantially higher stiffness than other lignocellulosic-based PU systems reported in the literature. The reduced elongation at break observed in the present materials reflects the formation of comparatively rigid macromolecular networks, highlighting the influence of lignin's typical chemical structure on the resulting polyurethanes' mechanical behavior. The rigid films can be used in applications where mechanical strength, dimensional stability, and low deformation are essential.

3.2.7. Scanning Electron Microscopy

Figure 11 shows micrographs of the cryofractured surfaces of the LignoPU$_{COPKL}$ and LignoPU$_{COPKL\text{-}Glu}$ series films, formed at 25 °C and 100 °C, respectively, the lowest and highest temperatures evaluated, which better reflect the observed differences.

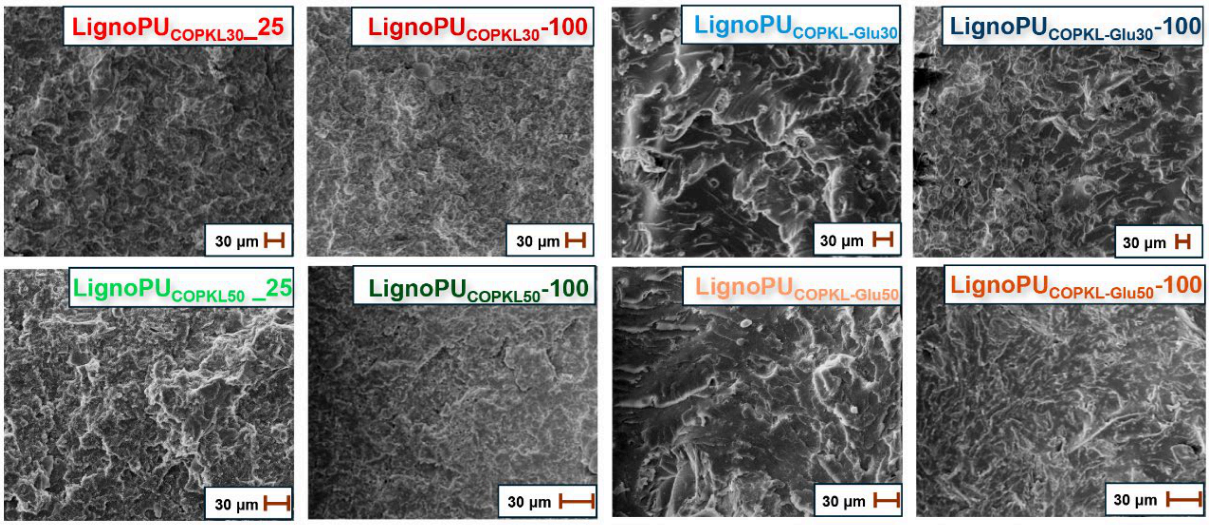


Figure 11. Scanning electron micrographs of the cryofractured surfaces of LignoPUs films prepared simultaneously with the synthesis carried out from CO, PKL or PKL-Glu (30 and 50%) and pMDI at 25 °C and 100 °C. **Note:** Data for LignoPU$_{COPKL30}$_25 and LignoPU$_{COPKL50}$_25 extracted from [19]. Reproduced with permission from Elsevier, order license ID 1785892-1.

Although the LignoPU$_{COPKL}$ series consists of films with different crystallinities (Table 6) and stiffness, as indicated by their respective Young's moduli (Figure 10e,f), it shows no significant differences in surface morphology. A similar behavior is observed in the LignoPU$_{COPKL\text{-}Glu}$ series. Conversely, the surfaces of the LignoPU$_{COPKL}$ series are predominantly rough, whereas those of the LignoPU$_{COPKL\text{-}Glu}$ series exhibit fracture surfaces with flat regions, particularly in LignoPU$_{COPKL\text{-}Glu30}$-25 and LignoPU$_{COPKL\text{-}Glu50}$-25 (Figure 11). This suggests that fracture type was dominated by segments present in the non-crystalline and crystalline regions, with larger segments derived from PKL-Glu largely defining the fracture type and the morphology of the fractured surfaces.

4. Conclusions

In this study, bio-based films were produced via PU synthesis using unmodified lignin (PKL) and ricinoleic acid triglyceride (the main component of CO) as hydroxyl sources, and the reactions were conducted at 50 °C, 75 °C, and 100 °C. In addition, glutaraldehyde-modified Kraft lignin (PKL-Glu) was used as a hydroxyl source; 30/70 and 50/50 ratios of PKL or PKL-Glu/CO were used. Reactions were conducted at 25, 50, 75, and 100 °C. In this scenario, the type of lignin used (PKL or PKL-Glu), the proportion of PKL or PKL-Glu, and the reaction temperature were considered to evaluate their impact on the properties of the films formed. In this context, the study deepened understanding of reactions with high renewable content, conducted without solvents or catalysts, to form biomass-derived polyurethane films. This alone underscores the study's significance in the ongoing search for processes and materials that align with sustainability principles.

Regarding general properties, films from the LignoPU$_{COPKL}$ and LignoPU$_{COPKL\text{-}Glu}$ series formed at 25 °C exhibited lower crystallinity than the others, showing a plateau starting at 50 °C, because the dense network of covalent and hydrogen bonds formed hindered the development of new crystalline regions. The lower crystallinity of films formed at 25 °C resulted in lower contact angles, whereas the other films were more hydrophobic; within the LignoPU$_{COPKL50}$ and LignoPU$_{COPKL\text{-}Glu50}$ series, the latter appeared more hydrophilic, suggesting polar groups oriented toward the surface.

Glass transition temperatures (Tgs) for both soft and hard domains were observed in most films; notably, films from the LignoPU$_{COPKL\text{-}Glu50}$ series were the only ones to exhibit soft-domain Tgs that increased with formation temperature: 87, 95, 146, and 169 °C for 25, 50, 75, and 100 °C, respectively. Furthermore, the hard-domain Tg was not detected in any film in this series, suggesting strong restriction of rigid-segment mobility.

All films in the LignoPU$_{COPKL50}$ and LignoPU$_{COPKL\text{-}Glu50}$ series exhibited higher tensile strength and significantly higher moduli than those in the LignoPU$_{COPKL30}$ and LignoPU$_{COPKL\text{-}Glu30}$ series. Overall, films from the LignoPU$_{COPKL\text{-}Glu50}$ series showed higher moduli than those from the LignoPU$_{COPKL\text{-}50}$ series, with the film formed at 100 °C standing out (tensile strength of 33 MPa, modulus of 1361 MPa). In general, films from the LignoPU$_{COPKL\text{-}Glu}$ series presented flat surfaces (indicative of homogeneous networks), whereas those from the LignoPU$_{COPKL}$ series exhibited rough surfaces (indicative of heterogeneous phase distribution).

The results showed that, during film formation, formulation and conditions can be controlled to balance crystallinity, hydrophobicity, and tensile properties, with PKL-Glu as a reagent enabling finer tuning of certain properties. LignoPU$_{COPKL\text{-}Glu}$ series films have potential for application testing in high-performance coatings requiring rigidity, in packaging materials with controlled hydrophilicity/hydrophobicity, and in the biomedical field, where adjustable Tgs are advantageous. LignoPU$_{COPKL}$ series films can be tested in applications requiring barrier properties, where a rougher morphology can increase tortuosity and diffusion resistance, as well as in applications requiring moisture control, which benefit from greater hydrophobicity.

Supplementary Materials: The following supporting information can be downloaded at https://www.mdpi.com/article/10.3390/biomass6050081/s1, Figure S1: FTIR spectra of the reaction mixtures (CO, PKL30%, and pMDI) in the region of 4000 to 650 cm^{-1}, immediately after deposition on the plate, and of the LignoPU$_{COPKL30}$ films formed at temperatures of (a) 25 °C, (b) 50 °C, (c) 75 °C, and (d) 100 °C; Figure S2: FTIR spectra of the reaction mixtures (CO, PKL-Glu30%, and pMDI) in the region of 4000 to 650 cm^{-1}, immediately after deposition on the plate, and of the LignoPU$_{COPKL\text{-}Glu30}$ films formed at temperatures of (a) 25 °C, (b) 50 °C, (c) 75 °C, and (d) 100 °C; Figure S3: FTIR spectra of the reaction mixtures (CO, PKL50%, and pMDI) in the region of 4000 to 650 cm^{-1}, immediately after deposition on the plate, and of the LignoPU$_{COPKL50}$ films formed at temperatures of (a) 25 °C, (b) 50 °C, (c) 75 °C, and

(d) 100 °C. Magnification of the 1600–1800 cm^{-1} region in c and d.; Figure S4: TG curves obtained for the series (a) $LignoPU_{COPKL30}$, (b) $LignoPU_{COPKL-Glu30}$, (c) $LignoPU_{COPKL50}$ and (d) $LignoPU_{COPKL-Glu50}$ formed at temperatures of 25 °C to 100 °C (N_2 atmosphere, flow rate: 50 mL min^{-1}, heating rate: 10 °C min^{-1}); Figure S5: dTG curves obtained for the series (a) $LignoPU_{COPKL30}$, (b) $LignoPU_{COPKL-Glu30}$, (c) $LignoPU_{COPKL50}$ and (d) $LignoPU_{COPKL-Glu50}$ formed at temperatures of 25 °C to 100 °C (N_2 atmosphere, flow rate: 50 mL min^{-1}, heating rate: 10 °C min^{-1}).

Author Contributions: A.R.C.: Conceptualization, Methodology, Formal analysis, Investigation, Data Curation, Writing—Original Draft, Writing—Review and Editing, Visualization; D.B.P.: Formal analysis, Writing—Original Draft, Writing—Review and Editing, Visualization; D.d.S.P.: Formal analysis, Writing—Original Draft, Writing—Review and Editing, Visualization; L.A.R.: Analysis TGA, DMA; E.F.: Conceptualization, Methodology, Formal analysis, Investigation, Resources, Writing—Original Draft, Writing—Review and Editing, Visualization, Project administration, Funding acquisition. All authors have read and agreed to the published version of the manuscript.

Funding: This study was supported by the National Council for Scientific and Technological Development, CNPq (EF, grant 409116/2025-4 and 309 226/2025-2), and the São Paulo Research Foundation, FAPESP (D.B.P, research fellowship, 2024-13189-9).

Data Availability Statement: All data generated or analyzed during this study are included in this published article and its Supplementary Information file.

Conflicts of Interest: The authors declare no conflicts of interest.

Abbreviations

The following abbreviations are used in this manuscript:

KL	Kraft Lignin
PKL	Purified Kraft Lignin
Glu	Gltaraldehyde
PKL-Glu	Hydroxyalkylated Purified Kraft Lignin
CO	Castor Oil
pMDI	Polymeric Methylene Diphenyl Diisocyanate
PU	Polyurethane
LignoPU	Lignocellulosic Polyurethane
NMR	Nuclear Magnetic Resonance
FTIR	Fourier Transform Infrared Spectroscopy
SEC	Size-Exclusion Chromatography
TGA	Thermogravimetric Analysis
TG	Thermogravimetric
dTG	Derivative Thermogravimetric
T_{onset}	Initial decomposition temperature
DMA	Dynamic Mechanical Properties
SEM	Scanning Electron Microscopy
$T_{Máx}$	Maximum loss rate temperature
Tg	Glass Transition
CA	Contact Angle

References

1. Li, Z.; Chen, K.; Wang, M. Green Materials for the Synthesis of Polyurethanes. In *Materials and Chemistry of Flame-Retardant Polyurethanes Volume 1: A Fundamental Approach*; American Chemical Society: Washington, DC, USA, 2021; pp. 37–58.
2. Elfahmy, H.; Elalami, D.; Oulkhir, A.; Lyamlouli, K.; El Ahmadi, Z. Sustainable Valorization of Sugarcane Bagasse Through Lignin Extraction, Bioethanol Production, and a Proof of Concept Lignin Application. *Biomass* **2026**, *6*, 55. [CrossRef]
3. Ramires, E.C.; de Oliveira, F.; Frollini, E. Composites based on renewable materials: Polyurethane-type matrices from forest byproduct/vegetable oil and reinforced with lignocellulosic fibers. *J. Appl. Polym. Sci.* **2013**, *129*, 2224–2233. [CrossRef]

4. de Oliveira, F.; Ramires, E.C.; Frollini, E.; Belgacem, M.N. Lignopolyurethanic materials based on oxypropylated sodium lignosulfonate and castor oil blends. *Ind. Crops Prod.* **2015**, *72*, 77–86. [CrossRef]
5. Arshanitsa, A.; Krumina, L.; Telysheva, G.; Dizhbite, T. Exploring the application potential of incompletely soluble organosolv lignin as a macromonomer for polyurethane synthesis. *Ind. Crops Prod.* **2016**, *92*, 1–12. [CrossRef]
6. Gadhave, R.V.; Mahanwar, P.A.; Gadekar, P.T. Lignin-Polyurethane Based Biodegradable Foam. *Open J. Polym. Chem.* **2018**, *8*, 1–10. [CrossRef]
7. Vale, M.; Mateus, M.M.; Galhano dos Santos, R.; Nieto de Castro, C.; de Schrijver, A.; Bordado, J.C.; Marques, A.C. Replacement of petroleum-derived diols by sustainable biopolyols in one component polyurethane foams. *J. Clean. Prod.* **2019**, *212*, 1036–1043. [CrossRef]
8. Safwan, M.R.; Abraham, S.; Charan, S.N.; Anbu, J. Characterization and performance evaluation of hydrophilic polyurethane foam for medical wound dressings. *Polym. Bull.* **2025**, *83*, 136. [CrossRef]
9. Ali, S.; Rani, A.; Dar, M.A.; Qaisrani, M.M.; Noman, M.; Yoganathan, K.; Asad, M.; Berhanu, A.; Barwant, M.; Zhu, D. Recent Advances in Characterization and Valorization of Lignin and Its Value-Added Products: Challenges and Future Perspectives. *Biomass* **2024**, *4*, 947–977. [CrossRef]
10. Dash, S.; Bhavanam, A.; Gera, P. Parametric optimization of kraft pulping of wheat straw for extraction of lignin using response surface methodology. *Biomass Convers. Biorefinery* **2024**, *14*, 18165–18182. [CrossRef]
11. Shorey, R.; Salaghi, A.; Fatehi, P.; Mekonnen, T.H. Valorization of lignin for advanced material applications: A review. *RSC Sustain.* **2024**, *2*, 804–831. [CrossRef]
12. Ma, X.; Chen, J.; Zhu, J.; Yan, N. Lignin-Based Polyurethane: Recent Advances and Future Perspectives. *Macromol. Rapid Commun.* **2021**, *42*, 2000492. [CrossRef] [PubMed]
13. Xie, Q.; Zhou, J.; Sun, H.; Fu, J.; Cui, M.; Wang, X.; Li, F.; Zhu, J.; Chen, J. Castor oil graphted lignin-based polyurethane film with excellent barrier properties. *Prog. Org. Coat.* **2026**, *211*, 109767. [CrossRef]
14. Jiang, X.; Liu, J.; Du, X.; Hu, Z.; Chang, H.; Jameel, H. Phenolation to Improve Lignin Reactivity toward Thermosets Application. *ACS Sustain. Chem. Eng.* **2018**, *6*, 5504–5512. [CrossRef]
15. Lisý, A.; Ház, A.; Nadányi, R.; Jablonský, M.; Šurina, I. About Hydrophobicity of Lignin: A Review of Selected Chemical Methods for Lignin Valorisation in Biopolymer Production. *Energies* **2022**, *15*, 6213. [CrossRef]
16. Goliszek, M.; Podkościelna, B.; Sevastyanova, O.; Fila, K.; Chabros, A.; Pączkowski, P. Investigation of accelerated aging of lignin-containing polymer materials. *Int. J. Biol. Macromol.* **2019**, *123*, 910–922. [CrossRef] [PubMed]
17. Watkins, K.; Fatehi, P. A review on lignin extraction processes at different production scales. *Ind. Crops Prod.* **2026**, *239*, 122526. [CrossRef]
18. Spada, J.C.; Lopes, A.A.; Barros, N.; Sarkis, J.R. Performance of kraft lignin as a filler in PLA composites via the acetic acid casting technique. *Polym. Bull.* **2025**, *82*, 2419–2439. [CrossRef]
19. Cassales, A.; Ramos, L.A.; Frollini, E. Synthesis of bio-based polyurethanes from Kraft lignin and castor oil with simultaneous film formation. *Int. J. Biol. Macromol.* **2020**, *145*, 28–41. [CrossRef] [PubMed]
20. de Paula, R.L.; Frollini, E. Progress in the synthesis of polyricinoleic acid via acid catalysis from the primary component of castor oil. *Biomass Conv. Bioref.* **2025**, *15*, 4647–4656. [CrossRef]
21. dos Santos, V.L.; dos Santos, L.C.L.; Simonelli, G. Transesterification of Castor Oil into Biodiesel: Predictive Modeling with Machine Learning and Genetic Algorithm. *Biomass* **2025**, *5*, 71. [CrossRef]
22. Chen, X.; Li, Z.; Zhang, L.; Wang, H.; Qiu, C.; Fan, X.; Sun, S. Preparation of a novel lignin-based film with high solid content and its physicochemical characteristics. *Ind. Crops Prod.* **2021**, *164*, 113396. [CrossRef]
23. Gao, S.; Zhao, J.; Yang, C.; Zhang, Y.; Fu, Y.; Zhang, A.; Yang, X.; Wang, Z.; Tian, G. Synthesis of lignin-based polyurethane (LPU) and fabrication of degradable mulch film through LPU coating on cellulose paper. *Ind. Crops Prod.* **2024**, *210*, 118099. [CrossRef]
24. Xue, B.-L.; Wen, J.-L.; Zhu, M.-Q.; Sun, R.-C. Lignin-based polyurethane film reinforced with cellulose nanocrystals. *RSC Adv.* **2015**, *4*, 36089–36096. [CrossRef]
25. Kim, B.; Lee, J.; Jang, S.; Park, J.; Choi, J.; Lee, S.; Jung, J.; Park, J. Exploring the Effect of the Polyol Structure and the Incorporation of Lignin on the Properties of Bio-Based Polyurethane. *Polymers* **2025**, *17*, 604. [CrossRef] [PubMed]
26. Tamantini, S.; Bergamasco, S.; Humar, M.; Petrič, M.; Romagnoli, M. A New Lignin-Based Polyurethane Film for Wood: Decay, Artificial Weathering, Physical and Morphological Characterization. *Molecules* **2025**, *30*, 4793. [CrossRef] [PubMed]
27. Bergamasco, S.; Tamantini, S.; Zikeli, F.; Vinciguerra, V.; Scarascia Mugnozza, G.; Romagnoli, M. Synthesis and Characterizations of Eco-Friendly Organosolv Lignin-Based Polyurethane Coating Films for the Coating Industry. *Polymers* **2022**, *14*, 416. [CrossRef] [PubMed]
28. Jia, Z.; Lu, C.; Zhou, P.; Wang, L. Preparation and characterization of high boiling solvent lignin-based polyurethane film with lignin as the only hydroxyl group provider. *RSC Adv.* **2015**, *5*, 53949–53955. [CrossRef]
29. Zhang, Y.; Wang, J.; Fang, X.; Liao, J.; Zhou, X.; Zhou, S.; Bai, F.; Peng, S. High solid content production of environmentally benign ultra-thin lignin-based polyurethane films: Plasticization and degradation. *Polymer* **2019**, *178*, 121572. [CrossRef]

30. da Silva, C.G.; Grelier, S.; Pichavant, F.; Frollini, E.; Castellan, A. Adding value to lignins isolated from sugarcane bagasse and *Miscanthus*. *Ind. Crops Prod.* **2013**, *42*, 87–95. [CrossRef]
31. Gordobil, O.; Moriana, R.; Zhang, L.; Labidi, J.; Sevastyanova, O. Assesment of technical lignins for uses in biofuels and biomaterials: Structure-related properties, proximate analysis and chemical modification. *Ind. Crops Prod.* **2016**, *83*, 155–165. [CrossRef]
32. Peralta, M.B.; Pajer, N.; Crestini, C.; Nicolau, V.V. Mechanistic insight into hydroxy-methylation of hardwood Kraft lignin. *Wood Sci. Technol.* **2024**, *58*, 2047–2072. [CrossRef]
33. Choi, J.W.; Faix, O. NMR study on residual lignins isolated from chemical pulps of beech wood by enzymatic hydrolysis. *J. Ind. Eng. Chem.* **2011**, *17*, 25–28. [CrossRef]
34. Gonçalves, A.R.; Schuchardt, U.; Bianchi, M.L.; Curvelo, A.A.S. Piassava fibers (*Attalea funifera*): NMR spectroscopy of their lignin. *J. Braz. Chem. Soc.* **2000**, *11*, 491–494. [CrossRef]
35. Gurunathan, T.; Mohanty, S.; Nayak, S.K. Isocyanate terminated castor oil-based polyurethane prepolymer: Synthesis and characterization. *Prog. Org. Coat.* **2015**, *80*, 39–48. [CrossRef]
36. Wang, C.; Ma, C.; Mu, C.; Lin, W. Tailor-made zwitterionic polyurethane coatings: Microstructure, mechanical property and their antimicrobial performance. *RSC Adv.* **2017**, *7*, 27522–27529. [CrossRef]
37. Dusek, K.; Spirkova, M.; Havlicek, I. Network formation of polyurethanes due to side reactions. *Macromolecules* **1990**, *23*, 1774–1781. [CrossRef]
38. Zharkov, V.V.; Vlasov, R.R. A quantitative study of the allophanate formation reaction in PIR foams by FT-IR spectroscopy. *J. Cell. Plast.* **2022**, *58*, 877–891. [CrossRef]
39. Chattopadhyay, D.K.; Webster, D.C. Thermal stability and flame retardancy of polyurethanes. *Prog. Polym. Sci.* **2009**, *34*, 1068–1133. [CrossRef]
40. Somani, K.P.; Kansara, S.S.; Patel, N.K.; Rakshit, A.K. Castor oil based polyurethane adhesives for wood-to-wood bonding. *Int. J. Adhes. Adhes.* **2003**, *23*, 269–275. [CrossRef]
41. Porto, D.S.; Cassales, A.; Ciol, H.; Inada, N.M.; Frollini, E. Cellulose as a polyol in the synthesis of bio-based polyurethanes with simultaneous film formation. *Cellulose* **2022**, *29*, 6301–6322. [CrossRef]
42. Oenema, J.; Liu, H.; De Coensel, N.; Eschenbacher, A.; Van de Vijver, R.; Weng, J.; Li, L.; Wang, C.; Van Geem, K.M. Review on the pyrolysis products and thermal decomposition mechanisms of polyurethanes. *J. Anal. Appl. Pyrolysis* **2022**, *168*, 105723. [CrossRef]
43. Morgado, D.L.; Frollini, E. Thermal decomposition of mercerized linter cellulose and its acetates obtained from a homogeneous reaction. *Polímeros* **2011**, *21*, 111–117. [CrossRef]
44. Corcuera, M.A.; Rueda, L.; Fernandez d'Arlas, B.; Arbelaiz, A.; Marieta, C.; Mondragon, I.; Eceiza, A. Microstructure and properties of polyurethanes derived from castor oil. *Polym. Degrad. Stab.* **2010**, *95*, 2175–2184. [CrossRef]
45. Trovati, G.; Sanches, E.A.; Neto, S.C.; Mascarenhas, Y.P.; Chierice, G.O. Characterization of polyurethane resins by FTIR, TGA, and XRD. *J. Appl. Polym. Sci.* **2010**, *115*, 263–268. [CrossRef]
46. Mishra, A.; Maiti, P. Morphology of polyurethanes at various length scale: The influence of chain structure. *J. Appl. Polym. Sci.* **2011**, *120*, 3546–3555. [CrossRef]

Disclaimer/Publisher's Note: The statements, opinions and data contained in all publications are solely those of the individual author(s) and contributor(s) and not of MDPI and/or the editor(s). MDPI and/or the editor(s) disclaim responsibility for any injury to people or property resulting from any ideas, methods, instructions or products referred to in the content.